
Doctoral Dissertations

Student Theses and Dissertations

1972

The use of shaped explosive charges to investigate permeability, penetration, and fracture formation in coal, dolomite and plexiglas

Calvin J. Konya

Follow this and additional works at: https://scholarsmine.mst.edu/doctoral_dissertations



Part of the [Mining Engineering Commons](#)

Department: Mining and Nuclear Engineering

Recommended Citation

Konya, Calvin J., "The use of shaped explosive charges to investigate permeability, penetration, and fracture formation in coal, dolomite and plexiglas" (1972). *Doctoral Dissertations*. 2083.

https://scholarsmine.mst.edu/doctoral_dissertations/2083

This thesis is brought to you by Scholars' Mine, a service of the Missouri S&T Library and Learning Resources. This work is protected by U. S. Copyright Law. Unauthorized use including reproduction for redistribution requires the permission of the copyright holder. For more information, please contact scholarsmine@mst.edu.

THE USE OF SHAPED EXPLOSIVE CHARGES TO
INVESTIGATE PERMEABILITY, PENETRATION, AND FRACTURE
FORMATION IN COAL, DOLOMITE AND PLEXIGLAS

by

CALVIN JOSEPH KONYA, 1943-

A DISSERTATION

Presented to the Faculty of the Graduate School of the

UNIVERSITY OF MISSOURI-ROLLA

In Partial Fulfillment of the Requirements for the Degree

DOCTOR OF PHILOSOPHY

in

MINING ENGINEERING

1972

T2749
112 pages
c. I

Ronald B. Rollins
Advisor

A. K. Rigler

R. J. Bruzeniski

Henry B. Leach

Robert W. Elles

ABSTRACT

The concentration of methane gas which exists in the exhaust air from a coal mine is critical. It can be controlled by dilution of the gas with fresh air or by the regulation of the rate of methane emission into the mine workings. Degasification techniques which control the emission rate are currently being developed. The use of shaped charges to initiate fractures in coal and increase the gas flow rate was the object of this research. The three areas of investigation were: 1) permeability changes in coal models after fracturing with shaped charge jets, 2) fracture formation in coal and other brittle materials, and 3) jet penetration capabilities of charges loaded with permissible explosives.

The first order penetration law, the Allison-Vitali equations, and their modification by DiPersio to account for continuous and broken jets have been used in attempts to predict jet penetration depth in metallic targets. Correction factors for the effects of material properties are used in these equations, but the specific properties which control the penetration rate were undefined and were investigated in this study.

The results of this research indicate that the permeability of coal can be increased for degasification purposes by the use of shaped charge jets. The fracture formation which resulted from the jet penetration was studied with radiographs and highspeed photography and indicated that longitudinal wave velocity, Young's modulus, and tensile strength are related to penetration depth.

ACKNOWLEDGMENT

The author wishes to express his gratitude to Dr. R. R. Rollins and Dr. G. B. Clark for their support and suggestions during this investigation.

He is also grateful to Mr. E. H. Roberts, Manager of Mines, Mr. R. Shockley, Mine Superintendent, and Mr. G. Zmudzinski, Safety Engineer for their assistance in obtaining coal samples from the Inland Steel Coal Mine in Sesser, Illinois.

Sincere thanks are extended to the United States Bureau of Mines for their financial support during this investigation.

TABLE OF CONTENTS

	Page
ABSTRACT	ii
ACKNOWLEDGMENT	iii
LIST OF ILLUSTRATIONS	vi
LIST OF TABLES	ix
I. INTRODUCTION	1
A. General	1
B. Nature of Investigation	5
II. PERMEABILITY OF ROCK MATERIALS	7
A. Darcy's Law	7
B. Gas Slippage Phenomenon	8
C. Permeability of Coal	9
III. THEORY OF JET PENETRATION	11
IV. EXPERIMENTAL RESULTS	15
A. Permeability Studies	15
1. Flow Rates In Block No. 1	15
2. Permeability of Small Samples	15
3. Permeability of Large Samples	18
B. Fracturing and Penetration	23
1. Plexiglas	25
2. Dolomite	36
3. Coal	40
4. Steel, Titanium, and Lead	55
C. Explosive Detonation Velocity	55
D. Jet Tip Velocity	57

Table of Contents (continued)	Page
V. DISCUSSION OF RESULTS	61
A. Permeability of Coal	61
B. Effects of Liner Material on Jet Penetration	65
C. Effects of Detonation Velocity on Jet Penetration	65
D. Effects of Material Properties on Jet Penetration	67
E. Shaped Charge Effects on Homogeneous and Bedded Targets	71
1. Stress Waves and Impulse Loads	72
a. Elastic Impact	72
b. Plastic Impact	73
c. Hydrodynamic Impact	73
2. Fracture Mechanics	74
3. Mechanics of Penetration in Coal	78
VI. CONCLUSIONS	80
BIBLIOGRAPHY	82
VITA	85
APPENDICES	
A. Experimental Design	86
B. Calculations for Sandstone Standard	99
C. Material Properties	102
D. Proximate Analysis of Coal From Illinois No. 6 Seam	103

LIST OF ILLUSTRATIONS

Figure	Page
1. Permeability of Sandstone Standard.....	17
2. Permeability Vs L_1/L in Coal (Parallel to Bedding).....	17
3. Permeability Vs L_1/L in Coal (Perpendicular to Bedding).....	24
4. Penetration of 60° Copper JRC in Plexiglas.....	26
5. Penetration Velocity for 60° and 100° Copper JRC in Plexiglas.....	28
6. Penetration Velocity for 100° Aluminum JRC in Plexiglas.....	28
7. Penetration Velocity for 80° Aluminum JRC in Plexiglas.....	29
8. Penetration Velocity for 100° JRC in Plexiglas.....	29
9. Jet Penetration Across Plexiglas Plates (100° Copper JRC).....	31
10. 10 Grain MDF Across Plexiglas Plates.....	32
11. Jet Penetration Parallel to Plexiglas Plates (100° Copper JRC).....	33
12. 10 Grain MDF Parallel to Plexiglas Plates.....	33
13. Jet Penetration for 100° Copper JRC at 45° to Plexiglas Plates.....	34
14. Penetration Velocity at 45° to Plexiglas Plates.....	35
15. Penetration Velocity for 100° Copper JRC Liners in Plexiglas.....	35

List of Illustrations (continued)	Page
16. Jet Penetration Profile in Plexiglas.....	37
17. Crater Profiles in Dolomite.....	41
18. Jet Penetration and Crater Depths in Dolomite.....	42
19. Jet Profile in Coal.....	44
20. Penetration Depth Vs Standoff Distance in Coal.....	46
21. Radiograph of 60° Copper JRC in Coal.....	47
22. Jet Penetration Velocity in Coal.....	48
23. Slugs from Shaped Charge Liners.....	51
24. Penetration in Dolomite.....	58
25. Penetration Depth Perpendicular to Coal Bedding (100° Copper JRC).....	59
26. Penetration Depth Perpendicular to Coal Bedding (60° Copper JRC).....	59
27. Jet Tip Velocity in Air (60° Copper JRC).....	60
28. Fracture Formation Parallel to the Bedding Due to Jet Penetration.....	62
29. Fracture Formation Perpendicular to the Bedding Due to Jet Penetration.....	63
30. Average Penetration Vs Target Density for 60° Copper JRC.....	68
31. Tensile Strength Vs Jet Penetration.....	68
32. Penetration Depth Vs Young's Modulus.....	70
33. Penetration Depth Vs Longitudinal Wave Velocity.....	70
34. Sample Holder for Large Specimens.....	89

List of Illustrations (continued)	Page
35. Sample Holder for Small Specimens.....	89
36. Diagram of Permeameter.....	91
37. Permeameter Assembly.....	92
38. Permeability Curve for Sandstone.....	101
39. Klinkenberg Correction for Sandstone.....	101

LIST OF TABLES

Table	Page
I. Permeability of Coal Samples Perpendicular to the Bedding Planes	19
II. Permeability of Coal Samples Parallel to the Bedding Planes	20
III. Permeability of Coal Blocks 1 Through 25	21
IV. Permeability of Coal Blocks 26 Through 42	22
V. Jet Penetration in Plexiglas	27
VI. Jet Penetration in Dolomite for 4.76 cm Diameter Charges	38
VII. Jet Penetration in Granite, Dolomite and Coal	39
VIII. Average Penetration in Coal by JRC Charges	45
IX. Penetration - Atlas 5Y	50
X. Penetration - Atlas 5U	52
XI. Penetration - Atlas Gelcoalite Z	53
XII. Penetration - DuPont 40% Special Gelatin	54
XIII. Penetration Data for Metallic Targets	56
XIV. Explosive's Properties	95
XV. JRC Charge Data	97
XVI. Penetration Tests in Steel for JRC Charges	98

I. INTRODUCTION

A. General

One of the oldest problems associated with the mining of coal is the emission of methane gas and the subsequent hazard of explosive concentrations accumulating in the mine workings.

Methane emission in coal mines is governed by two distinct processes which can be broken down into flow through the micropore structure and flow through the fracture system.

Gas transport through the micropore structure is governed by Fick's law of diffusion (1):

$$Q = DA \frac{dC}{dL} \quad (I-1)$$

where

Q = volume flow rate

D = diffusion coefficient

A = cross sectional area

C = gas concentration in solid coal

L = length

Coal is a porous material with a pore diameter on the order of 4 or 5 angstroms (2). The pores are classified as dispersed or connected (3). Dispersed pores have little interconnection and flow from pore to pore is difficult if not impossible. Connected pores allow gas to flow easily through the material. Material having a small connected pore porosity has a greater permeability than material with dispersed pores of a higher porosity.

The majority of pores in an average coal sample are those of the dispersed type. For this reason two coal samples of the same

volume but of different size distributions can vary greatly in methane emission per unit time. Fine coal dust (275 to 325 mesh) saturated with adsorbed methane at 15 psi gage will release all its methane in 30 minutes while one-quarter-inch coal under the same conditions will require 30 days to release all of its methane (2). The amount of methane which can be adsorbed and stored can be as much as 2000 cubic feet per ton (1). This methane can be quickly released by degradation of the coal into fine dust. The methane release would be proportional to the amount of new surface area exposed by the degradation. The concentration gradient acts as the driving force for interpore flow (4).

Gas flow through fractures in the coal, which is the only mechanism rapid enough to be of importance in in situ degasification, is governed by Darcy's law (5):

$$Q = \frac{k A dP}{\mu dL} \quad (I-2)$$

where

Q = volume flow rate through sample

k = permeability

μ = gas viscosity

A = cross sectional area of sample

P = pressure

L = length of flow path through sample

The driving force for flow through the fractures is the pressure gradient.

Methane emission into a mine and methane movement through a seam are dependent on the degree of metamorphism the seam has undergone and other factors such as depth of burial and geological

features such as joints, mud seams and partings.

Methane pressure in some virgin coal seams can be as high as 550 psi at less than 200 feet from the working face (5). In such situations the fracture permeability is very low. In another coal seam where the fracture permeability is high the gas may migrate at flow rates as high as 13 feet per minute and gas flow from distances of 800 feet have been reported (6).

These two modes of gas flow are different but they are interdependent. The equilibrium quantity of gas contained in the micropore structure is directly proportional to the gas pressure in the fracture system according to the empirical relationship (1):

$$C_0 = bP^n \quad (I-3)$$

where

C_0 = equilibrium quantity of adsorbed gas per unit weight of coal

P = pressure

b and n are constants

Two conditions must be satisfied in order to have gas migration over a relatively long distance. A large fracture density must be accompanied by a large fracture permeability. If only one of the above conditions exist, then the mass transport mechanism will change to diffusion rather than flow through the fractures.

Methods of degasification tried in the United States consist of the following basic methods and modifications of each.

1. Surface and underground boreholes
2. Water infusion

3. Foam infusion

4. Underground blocking methods

The above methods help to control the rate of methane emission in permeable coal deposits. Geologic features such as mud seams and partings can completely seal a portion of the seam such that the above methods will not work and little or no gas will migrate across these geologic discontinuities. These portions of the seam will retain their high methane content until mined (6). The use of explosives to fracture geologic formations may be an answer to this problem. Explosives may also help increase gas flow through seams where fracture density is large but fracture permeability is small.

Conventional explosive charges have been used in attempts to increase the gas liberation rate. The energy from conventional charges moves out spherically and local crushing results around the charge which has a detrimental effect on gas flow. In 1960, Ammosov (7) concluded that the presence of exogenetic shear fractures, such as those which result from compression normal to the bedding, cause blockage of the flow channels and actually lower the permeability.

The use of shaped charges with lined or unlined cavities can offer the necessary fracturing and directionality of fracturing without the crushing which results from conventional charges. Shaped charges are those types of explosive devices where the explosive energy is not uniformly distributed spherically around the charge but because of charge geometry the energy output in one specific direction is increased. Shaped charges having a cavity

opposite the point of initiation are effective in increasing breakage in this one direction. This effect known as the cavity effect or Monroe effect as it is called in the United States was first described by Charles Monroe in 1888. R. W. Woods is credited by Eichelberger (8) for the recognition of the benefits of lining the shaped charge cavity with a metallic liner. This liner greatly increased the penetration capabilities of shaped charges over those obtained using only the Monroe effect. The high velocity fragments from the metal liners cause the increased penetration capabilities of lined shaped charges.

Since their advent, metal lined shaped charges have found extensive use in military applications such as penetration of high strength steel. Commercial applications are limited to tapping blast furnaces and perforating oil well casings. A great deal of information is available on the penetration of metallic targets by metallic jets but because of their limited commercial use little information is available on the penetration of metallic jets in other target materials. The effect of lined cavity charges on rock was investigated by Clark (9), Austin (10), Hutt1 (11) and Kalia (12). These investigators studied shaped charge effects on breaking concrete, rhyolite, limestone and granite blocks.

B. Nature of the Investigation

The primary objective of this research was to determine the effects shaped charge induced fractures had on the permeability of coal. This was accomplished by investigating the effects of the following:

- a) Four different liner materials
- b) Six different explosives, three of which were permissibles
- c) Three different target materials which exhibit brittle failure
- d) Permeability measurement on large and small coal samples

II. PERMEABILITY OF ROCK MATERIALS

A. Darcy's Law

Permeability measuring procedures on rock have been well developed by the petroleum industry. The American Petroleum Institute has a standard procedure (13) which has been accepted for use by the industry. This procedure has been followed for this study.

The standard Darcy equation for gases (13) may be written

$$k = \frac{\mu Q_A V L}{A(P_1 - P_2)} \quad (\text{II-1})$$

The standard unit for k is the darcy. The units for the above equation are

$$\text{darcy} = \frac{(\text{cp}) (\text{cm}^3/\text{sec.}) (\text{cm})}{(\text{cm})^2 (\text{atmos.})}$$

where

cm = centimeters

cp = centipoise

sec. = seconds

atmos. = atmospheres

The above equation is valid subject to the following limitations

(1).

1. The flowing fluid is an inert homogeneous gas.
2. The flow must be laminar.
3. The effect of gas slippage is taken into consideration.

B. Gas Slippage Phenomena

Air is commonly used as the flowing fluid for determination of permeability. The air permeability values, however, do not agree with those determined with gases such as hydrogen or carbon dioxide (14) and none of the above agree with the values obtained by using water (3). Klinkenberg (15) proved that the discrepancies in gas permeability and liquid permeability are due to gas slippage, a well-known phenomenon related to gas flow in capillary tubes.

Fulton (16) states that in the viscous flow of a fluid through a capillary, the velocity of a thin layer of fluid adjacent to the walls of the capillary is theoretically zero, but when the ratio of the radius of the capillary to the mean free path of the gas is such that intermolecular collisions decrease, then the molecular collisions with the walls increase in importance. The thin layer of zero velocity gas may lose its attachment to the capillary surface and will have a finite velocity. Gas slippage occurs when the diameter of the capillary openings approach that of the mean free path of the gas molecules. The mean free path is a function of molecular size and kinetic energy. The observed permeability to gas approaches a limiting value as the reciprocal mean pressure approaches infinity, i.e., at the value for liquid permeability. The Klinkenberg equation is (15):

$$K_L = \frac{K_G}{1 + \frac{b}{p_M}} \quad (\text{II-2})$$

where

K_L = permeability of the medium to a single phase liquid at constant temperature

K_G = permeability of the medium to a gas at constant temperature

P_M = mean pressure at which the gas is flowing

b = constant (Klinkenberg) for a given gas and a given medium

If the Klinkenberg extrapolation technique is not used, the resulting gas permeabilities may be too high. As capillaries increase in size, the percentage error in Darcy's equation decreases. For a permeability of 0.5 millidarcys errors may be in excess of 100 percent, while for permeabilities of 100 millidarcys the error is about 5 percent. For practical problems such as sampling a petroleum reservoir the permeability to gas (air) at low pressure is taken as the single-valued permeability of a nonreactive porous material to fluids (air, water) with the error well within the statistical and experimental error from other causes (1). Steward (17, 18) states that the slippage effect in a heterogeneous porous limestone had no measurable effect on permeability measurements because the hairline fracture width was large compared to the molecular mean free path of the gas molecules.

C. Permeability of Coal

Flow through fracture systems of the coal is the primary type of mass transport of methane in coal beds in the United States, and initial investigations have been made to evaluate some of the parameters involved (19, 20, 21, 22, 23).

Diffusion studies of gases through coal have been conducted by a number of investigators (1, 4, 9, 24, 25, 26, 27). Karn (25) found the diffusion rate across the bedding to be one-third to

one-half that along the bedding. Gas flow along the bedding was reported to be $1.20 \times 10^{-10} \text{ cm}^2 \text{ sec}^{-1} \text{ atm}^{-1}$ and 0.56×10^{-10} across the bedding. Sevenster (4) reported flows of $0.28 \times 10^{-10} \text{ cm}^2 \text{ sec}^{-1} \text{ atm}^{-1}$ without specifying bedding orientation. The coal samples for both studies were from different locations which could account for the different values. These flow rates are low in comparison to those observed in samples of larger dimensions, which supports the conclusion that diffusion is not the primary mode of gas transport through the coal seam. In situ investigations of methane flow rates have been performed (4, 28, 29) but these do not define the permeability of the seam because neither the cross sectional flow area nor the flow path length is known.

III. THEORY OF JET PENETRATION

The effect of jets from shaped charges on metallic targets and the parameters which effect penetration have been investigated and a wealth of information is available on the subject. Cone collapse phenomena are well documented in the literature and a good review of the subject is given by Cook (30).

The first order penetration law was developed from the Bernoulli theorem. The jet penetration is given by:

$$P_d = L \left(\frac{\rho_j}{\rho_t} \right)^{\frac{1}{2}} \quad (\text{III-1})$$

where

P_d = penetration depth

L = jet length

ρ_j = jet density

ρ_t = target density

Equation (III-1) was derived by assuming that the pressure of the impinging jet exceeds the strength of the target and the penetration process is hydrodynamic in character, with incompressibility of jet and target also being assumed. Empirical corrections factors have been used by many investigators to explain effects of target strength, jet breakup, and standoff relationships. This equation indicates, however, that the depth of penetration is independent of jet velocity and as derived does not account for the strength of target materials.

Allison-Vitali (31) adopted the hydrodynamic approach and considered the jet particles after jet breakup to be short steady state jets. The penetration of the jet was assumed completed at some

minimum velocity which was dependent on the strength properties of the target (Equation III-2). The use of the equation in this form is difficult because of the inability to determine the jet length (L).

$$P_d = \int_{t_0}^T U dt = \int_0^L U \frac{dl}{V-U} = \frac{1}{\gamma} \int_0^L dl = \frac{L}{\gamma} \quad (\text{III-2})$$

where

P_d = total penetration

L = total length of penetrating jet

U = velocity of penetration

V = jet tip velocity during penetration

$dl = (V-U) dt$ is jet length producing penetration in time dt

$V-U$ = relative velocity of approach of jet to target

$T-t_0$ = total penetration time

$$\gamma = \sqrt{\frac{\rho_t}{\rho_j}}$$

DiPersio (31) modified the Allison-Vitali equation to account for:

a) continuous jets, b) partially continuous jets, and c) completely broken jets. The three forms of the penetration equations are:

$$a) P_d = Z_0 \left[\frac{V_j^0}{(1+\gamma)U^{MIN}} \right]^{1/\gamma} - 1 \quad (\text{III-3})$$

$$b) P_d = \frac{(1+\gamma) (V_j^0 t_1)^{\frac{1}{1+\gamma}} Z_0^{\frac{\gamma}{1+\gamma}} - V_j^{MIN} t_1}{\gamma} - Z_0 \quad (\text{III-4})$$

$$c) P_d = \frac{\left[V_j^0 - V_j^{MIN} \right] t_1}{\gamma} \quad (\text{III-5})$$

where

P_d = total penetration depth

Z_0 = distance from the virtual origin of the jet to the front surface of the target

V_j^0 = jet tip velocity in flight (constant)

V_j^{MIN} = minimum velocity of jet particle capable of contributing to penetration into a target of given hardness (constant)

t_1 = jet breakup time assuming jet originates at the virtual origin at time zero

$$\gamma = \sqrt{\frac{\rho_t}{\rho_j}}$$

Pack (32) independently corrected the first order penetration law for the strength properties of the target. He considered the jet penetration as a series of powers of the nondimensional parameter $Y/\rho_t V^2$, and modified the equation to be:

$$\frac{P_d}{L} = \left[\frac{\rho_j}{\rho_t} \right]^{\frac{1}{2}} \left[1 - \frac{Y \alpha_1}{\rho_j V^2} \right] + \frac{r}{L} \quad (\text{III-6})$$

where

Y = dynamic yield strength of the target

α_1 = empirical function of the densities of the jet and target

V = jet velocity

r = radius of the hole made by the jet

The first order penetration law and its modifications explain jet penetration and hypervelocity projectile impact over a range of metallic target properties, yet when materials with considerably

different properties are used as the target, the law fails to accurately predict penetration results. Because of the lack of adequate theories, many attempts were made to correlate experimental data. Pugh and Eichelberger (33) were first to introduce the effect of strength through the use of the Brinell Hardness number to hypervelocity penetration. Other authors have used sonic velocities, yield strength, Brinell hardness and other physical properties of the target to validate existing penetration equations.

Clark (9), Austin (10), Hutt1 (11), and Kalia (12) have investigated the penetration of rock materials by metallic jets with the conclusion that metals which behave in a ductile fashion give the best penetration in rock. Brass and copper liners with apex angles between 40 and 60 degrees penetrate best in both metallic and nonmetallic targets. Shaped charge jet penetration in brittle materials cause large radial fractures to form, the extent of which are presently unknown. Large fractures induced in coal by jet penetration would be beneficial for degasification purposes.

IV. EXPERIMENTAL RESULTS

A. Permeability Studies

1. Flow Rates in Block No. 1 (Experimental design, Appendix A)

Dimensions of block No. 1 were 27.3 by 27.3 by 30.4 cm high. The sample was sealed into the permeability chamber with the top and bottom surfaces left open to permit gas flow. The specimen was oriented to test the flow of gas along the bedding planes. The rate of flow out of the face was $315 \text{ cm}^3/\text{sec}$ with a pressure gradient across the sample of 2 atmospheres. The chamber was designed so that gas flow rates for the sealed faces could also be measured. Holes 1.27 cm in diameter and 1.0 cm deep were drilled through the wax into the coal. Gas was introduced into the top of the vessel and flow rates along and across the bedding were measured at the four side openings. The gas flow rates measured along the bedding were 145 and $82 \text{ cm}^3/\text{sec}$ while flow rates across the bedding were 30 and $115 \text{ cm}^3/\text{sec}$. This variation of flow rates in the same bedding orientation indicates that the geologic features influence flow rates more than the micropore structure of the coal.

2. Permeability of Small Samples

A homogeneous core of sandstone was cut into a 3.2 cm cube and encased on four sides in "Quickmount," a quick setting epoxy resin. The epoxy bonded well to the rock and provided the necessary confinement on four sides of the sample which served as a standard to calibrate the permeability apparatus. The standard was tested under three conditions, permeability graphs were drawn, and corrections

made for the Klinkenberg effect (Appendix B). The experimental conditions were: 1) the specimen was moistened and placed in a 100% relative humidity environment for one week at 24°C, 2) it was oven dried for three days at 104°C, and 3) it was air dried for three weeks at about 60% relative humidity and 24°C. The permeability function for the two phase system (air-moisture) is curved rather than a straight line (Fig. 1). The slopes of the room temperature and oven dried permeability curves are essentially the same. The oven dried sample had an air permeability of 745 millidarcys, while the Klinkenberg corrected value for the permeability was 725 millidarcys. Based on these results and the small error introduced by omitting the Klinkenberg correction (2.8 percent), the coal block permeabilities were measured under ambient conditions on the as received coal blocks.

Natural fractures in the coal seam are of two basic types, those formed during the coalification process and those formed by outside tectonic forces acting on the coal bed. Tectonic forces are responsible for the major and minor cleavage planes (cleats) in the coal. The permeability of 32 small coal samples was tested to determine the percentage of gas which flows through the major joints and cleats and the percentage through the microfractures. The samples were approximately 1.27 cm cubes, cast in Quickmount, with the exposed faces machined parallel on a surface grinder. Twenty-five samples were cast in each bedding orientation in order to determine the effect of the bedding on flow through the microfracture system. Samples were selected such that only those without visible cleavage planes were tested for permeability. The average permeability

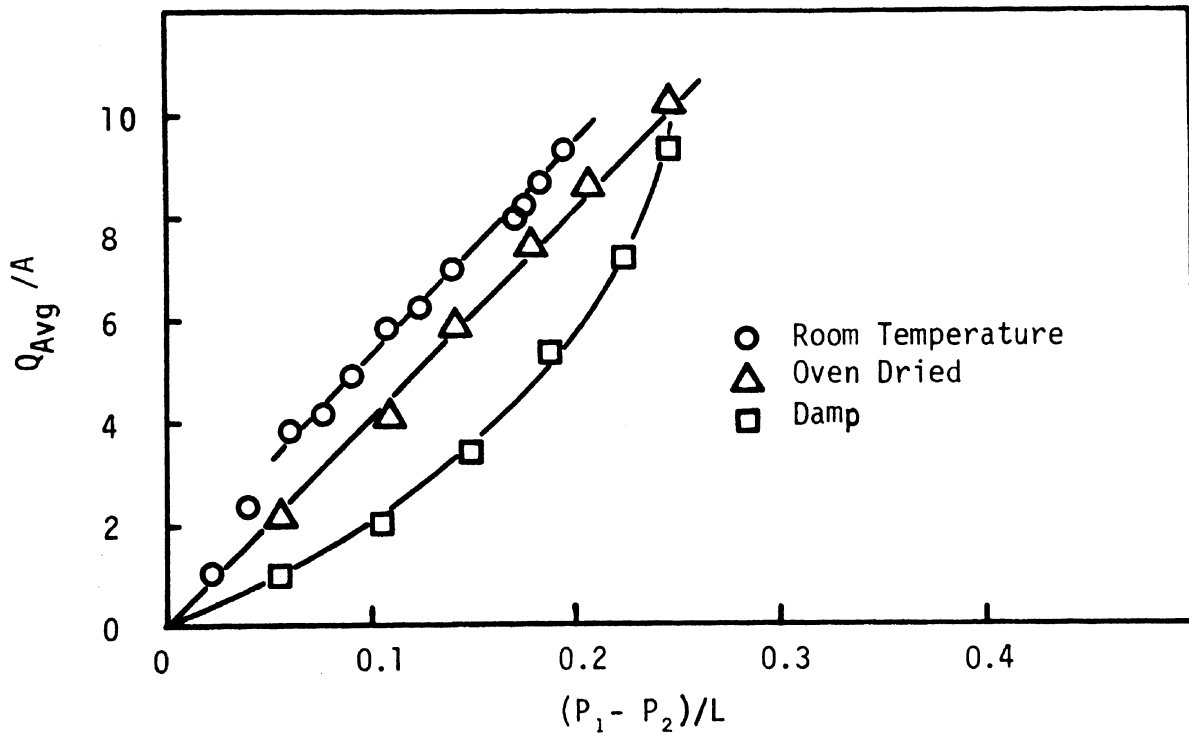


Figure 1. Permeability of Sandstone Standard

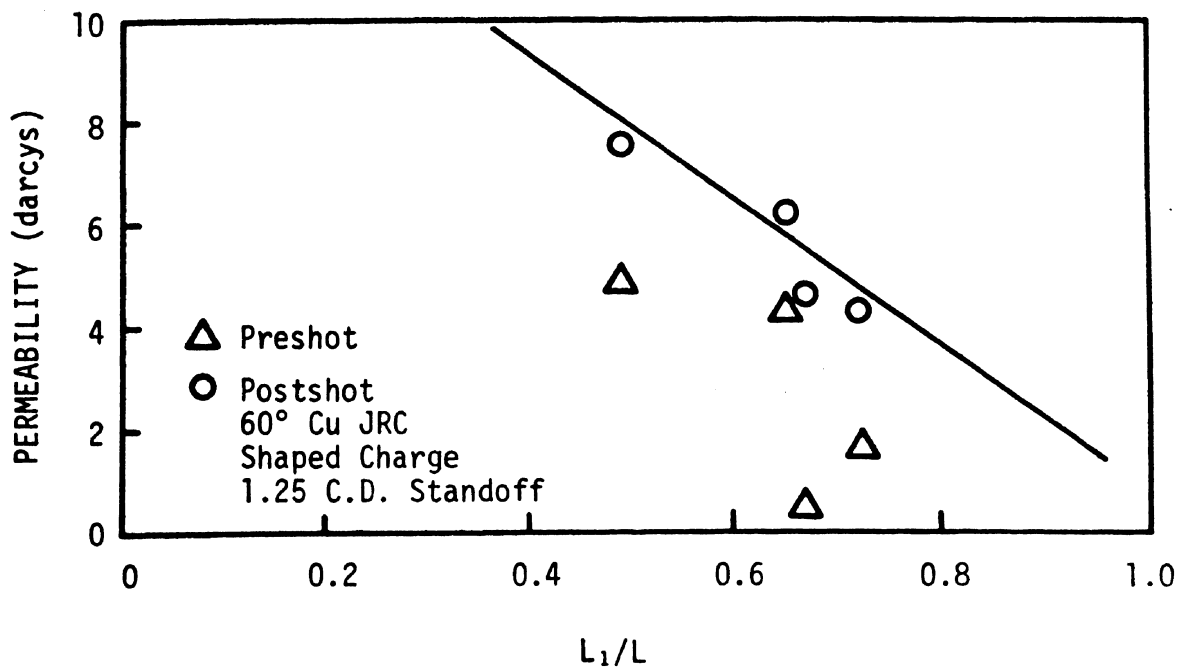


Figure 2. Permeability Vs L_1/L in Coal (Parallel to Bedding)

across the bedding was 0.014 millidarcys (Table I) while the flow along the bedding was 0.348 millidarcys (Table II), which confirms that the flow of gas through the microfracture systems and along the bedding planes is the dominant mode of gas migration rather than across the strata. Microscopic examination of the coal surfaces verified that the number of fractures oriented parallel to the bedding planes was much greater than in the perpendicular direction. The gas flow rate was measured in both the forward and reverse directions on samples parallel to the bedding, which in some cases gave a different permeability value, indicating preferred directions of flow.

3. Permeability of Large Samples

The preshot permeability of the coal sample was determined in one direction. The gas flow was reversed in the same bedding orientation and the permeability was recalculated. The two permeability measurements differed for many samples from the first group of coal specimens. The first group of samples, 5 thru 25, were taken from a syncline, where the strata was dipping inward toward a central basin, and contained a greater joint frequency than the flat lying portions of the seam. Samples 5 thru 25 indicated a preferred direction of flow, which was not evident in samples 26 thru 42 which were obtained from a different face in the mine. The preshot permeabilities seemed to be randomly distributed (Tables III and IV), which would be expected because permeability is not only dependent on the fracture density but also on the continuity of these fractures.

Jet penetration depth into the sample influences the length of

TABLE I
PERMEABILITY OF COAL SAMPLES PERPENDICULAR TO THE BEDDING PLANES

<u>Sample Number</u>	<u>Area (cm²)</u>	<u>Length (cm)</u>	<u>Permeability (millidarcys)</u>
C-2	2.25	1.4	0.0018
C-3	2.56	1.3	0.0000
C-6	1.44	1.0	0.475
C-8	1.82	1.0	0.0000
C-10	1.82	1.2	0.0000
C-11	1.56	0.9	0.0000
C-14	1.80	1.1	0.0000
C-15	1.43	1.0	0.0000
C-16	1.69	1.3	0.1097
C-17	1.32	1.2	0.0000
C-18	1.68	0.9	0.0000
C-19	1.82	1.3	0.0549
C-20	1.82	1.1	0.0000
C-22	1.56	1.0	0.0000
C-23	1.68	1.2	0.0000

Note: Air permeability values with no Klinkenberg correction

TABLE II

PERMEABILITY OF COAL SAMPLES PARALLEL TO THE BEDDING PLANES

<u>Sample Number</u>	<u>Area (cm²)</u>	<u>Length (cm)</u>	<u>Permeability Normal (millidarcys)</u>	<u>Permeability Reverse (millidarcys)</u>
C-25	1.821	1.11	0.8230	0.8230
C-28	2.041	1.11	0.2744	0.3109
C-29	1.815	1.11	0.0000	0.0000
C-30	1.815	1.11	0.0000	0.1280
C-31	1.928	1.11	0.5669	0.6219
C-32	2.13	1.14	0.5487	0.5487
C-33	1.94	1.14	0.6035	1.0059
C-34	1.77	1.14	0.0000	0.0000
C-35	1.77	1.14	0.0000	0.0000
C-36	1.77	1.14	0.0000	0.0000
C-37	1.77	1.14	0.2377	0.2377
C-38	1.61	1.14	0.0915	0.1829
C-39	1.95	1.14	0.4938	0.6767
C-40	1.77	1.14	0.5121	0.6584
C-41	1.95	1.14	0.4938	0.4938
C-45	1.88	1.14	0.3475	0.4572
C-46	1.93	1.14	0.2377	0.5304
C-47	1.61	1.14	0.3292	0.3292

Note: Air permeability values with no Klinkenberg correction

TABLE III
PERMEABILITY OF COAL BLOCKS 1 THROUGH 25

Block Number	Area (cm ²)	Length (cm)	Bedding Orientation	Permeability		Permeability		Liner Angle (deg)	Liner Material	Penetration (CD)	Standoff (CD)
				Preshot Normal (darcys)	Preshot Reverse (darcys)	Postshot Normal (darcys)	Postshot Reverse (darcys)				
1	--	--	along	--	--	--	--	100	Cu	--	1.25
2	--	--	across	--	--	--	--	100	Cu	8.0	1.25
3	--	--	along	--	--	--	--	100	Cu	8.0	1.25
4	--	--	across	--	--	--	--	100	Cu	7.0	1.25
5	--	--	across	--	--	--	--	100	Cu	8.0	1.25
6	--	--	along	--	--	--	--	60	Cu	12.0	1.25
7	--	--	across	--	--	--	--	100	Cu	6.0	1.25
8	413	14.0	across	1.170	1.170	2.850	2.850	60	Cu	11.0	1.25
9	613	21.6	across	1.280	0.585	9.570	9.570	60	Cu	9.0	1.25
10			along					100	Ti	1.5	1.25
11	439	22.9	along	0.384	1.335	4.700	4.700	60	Cu	12.0	1.25
12	323	15.2	across	2.469	6.986	4.974	5.340	60	Cu	8.5	1.25
13	448	23.5	along	4.792	8.176	7.627	9.346	60	Cu	9.0	1.25
14	387	26.7	along	5.230	7.243	4.180	3.548	100	Al	9.25	2.25
15	448	25.4	along	5.907	9.620	4.060	3.658	100	Al	7.5	2.25
16	310	25.4	across	8.176	7.407	11.614	11.614	100	Al	7.5	2.25
17	548	17.8	across	2.944	2.944	5.725	3.109	80	Al	7.0	2.25
18	232	24.8	along	1.829	2.743	5.715	5.715	80	Al	8.5	2.25
19	329	19.1	across	4.902	4.902	7.316	6.584	80	Al	7.25	2.25
20	339	24.1	across	14.028	14.028	17.869	10.261	100	Cu	7.25	1.25
21	413	24.8	across	3.841	3.841	6.529	8.743	100	Cu	6.5	1.25
22	316	24.8	across	1.353	2.286	10.059	10.059	100	Cu	5.5	1.25
23	328	18.4	across	5.926	7.188	19.442	10.059	100	Cu	7.5	1.25
24	436	25.4	across	6.010	5.395	8.486	10.370	100	Cu	6.25	1.25
25	169	19.7	along	3.493	3.493	12.254	12.254	100	Cu	6.5	1.25

TABLE IV
PERMEABILITY OF COAL BLOCKS 26 THROUGH 42

Block Number	Area (cm ²)	Length (cm)	Bedding Orientation	Permeability		Permeability		Liner Angle (deg)	Liner Material	Penetration (CD)	Standoff (CD)
				Preshot Normal (darcys)	Preshot Reverse (darcys)	Postshot Normal (darcys)	Postshot Reverse (darcys)				
26	429	18.42	across	1.682	1.682	1.770	1.770	100	Cu	7.2	1.25
27	542	19.05	across	3.109	3.109	3.402	3.402	100	Al	6.8	2.25
28	413	17.78	across	4.572	4.572	3.365	3.365	100	Al	4.0	2.25
29	581	14.73	across	4.188	4.188	2.725	2.725	80	Al	9.0	2.25
30	377	25.40	along	7.609	7.609	7.609	7.609	100	Cu	9.6	1.25
31	377	18.42	along	8.633	8.633	8.633	8.633	100	Cu	8.2	1.25
32	232	18.73	along	7.225	7.225	9.145	9.145	100	Al	6.6	2.25
33	234	24.13	along	12.855	19.259	21.691	21.691	80	Al	6.6	2.25
34	348	25.40	along	13.990	13.990	13.990	13.990	80	Al	8.0	2.25
35	362	19.05	along	10.041	10.041	8.231	8.231	60	Cu	7.0	0.25
36	362	19.05	along	4.295	4.295	6.182	6.182	60	Cu	9.8	0.25
37	515	19.56	along	1.769	1.769	4.340	2.613	60	Cu	11.2	0.25
38	298	20.07	along	5.167	5.167	8.633	8.633	80	Al	4.0	0.25
39	311	19.56	along	9.236	9.236	6.559	6.559	80	Al	2.8	0.25
40	364	19.68	along	5.219	5.219	3.886	3.886	80	Al	3.0	0.25
42*	872	29.21	across	2.360	2.360	1.541	1.541	20	Brass	2.4	0.00

*Brass liner 1.0 in. diameter.

the gas flow path, but in the Darcy equation the pressure gradient is divided by the total sample length, which disregards the jet penetration depth. To normalize the effect of the jet penetration, the permeability was plotted as a function of L_1/L where L_1 is the depth of penetration and L is the total sample length.

The data for all liner materials and angles except the 60° copper cone showed considerable scatter. The postshot permeability of samples fractured by jets from 60° copper liners was linearly related to L_1/L , in shots both parallel and perpendicular to the bedding (Figs. 2 and 3). The empirical equation is of the form

$$k = -15 L_1/L + C \quad (\text{IV-1})$$

where

k = permeability in darcys

L_1 = depth of jet penetration

L = length of sample

$C = 16.0 \pm 0.5$

B. Fracturing and Penetration

Penetration of shaped charge jets and resultant fracture formation were studied in three brittle materials and three ductile materials (Appendix C). Because of the heterogeneity and bedding planes of coal, numerous shots are necessary to define the effects of shaped charges of different liner materials and varying liner angles. For these reasons experiments were performed in Plexiglas, where visual observations could be made, and dolomite, which was readily available, as well as in coal. Jet penetration data were

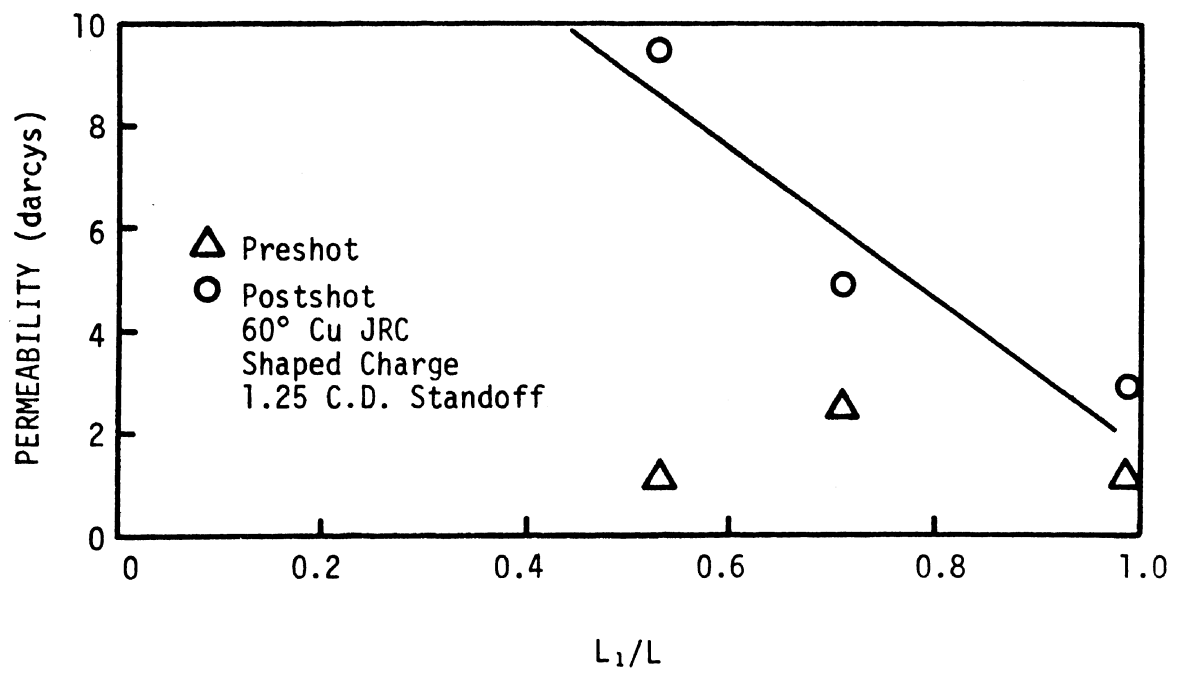


Figure 3. Permeability Vs L_1/L In Coal (Perpendicular to Bedding)

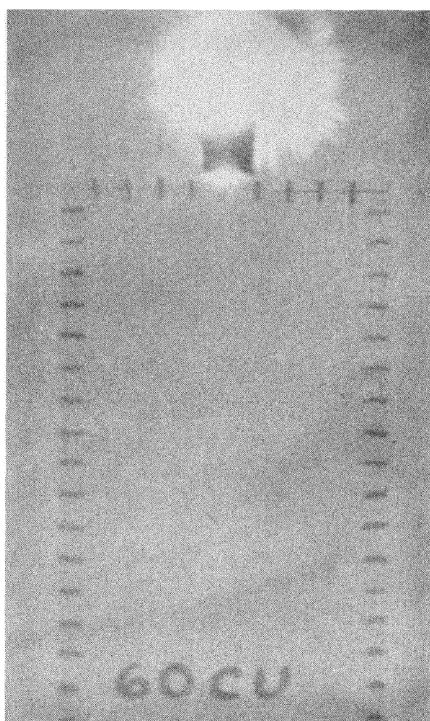
also obtained for steel, titanium and lead to compare penetration results in both ductile and brittle target materials and to confirm the penetration depth versus tensile strength relationship that was observed.

1. Plexiglas

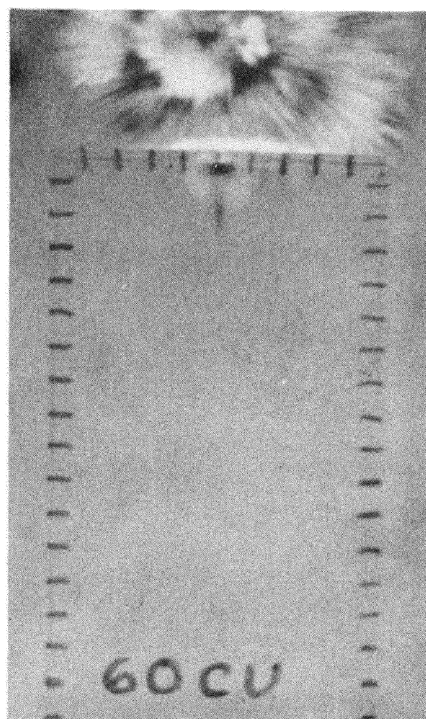
Models of Plexiglas were photographed (Fig. 4) during the jet penetration process and fracture and jet velocities were calculated (Table V). The jets from 60° copper liners exhibited a greater initial penetration velocity than those from 100° copper liner (Fig. 5), while the change in jet velocity as related to penetration distance was greater for jets from the 100° copper liners. The majority of the fractures caused by impact and stagnation pressure of the jet were complete in less than 100 μ sec.

Aluminum liners with 100° apex angles were photographed utilizing standoffs of one and two cone diameters (CD) (Fig. 6) and charges fired at a 2 CD standoff produced jets with both the highest initial penetration velocity and the greatest total penetration.

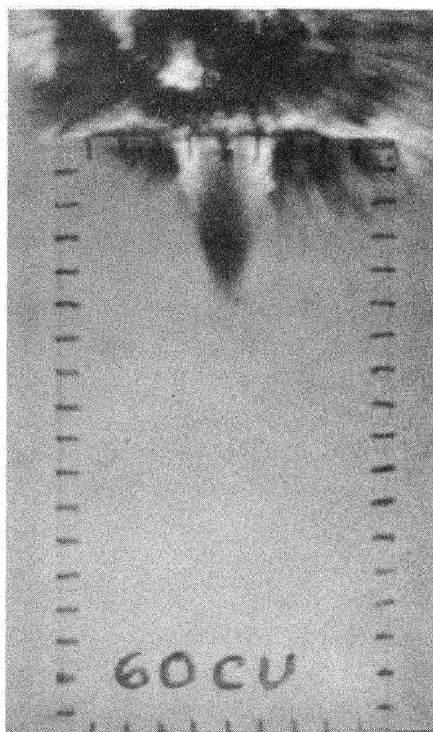
Jets from 80° aluminum liners fired at 1 and 2 CD standoffs showed trends similar to those observed in 100° aluminum liners except that the initial penetration velocity was greater for the 80° liner with a 2 CD standoff (Fig. 7). Penetration velocities from the 100° and 80° aluminum liners at one CD standoff were identical. A comparison of the effect of liner material on penetration velocity (Fig. 8) of jets from 100° liners of the same geometry and the same standoff shows that titanium had the highest initial penetration with lower values for aluminum and copper. Titanium



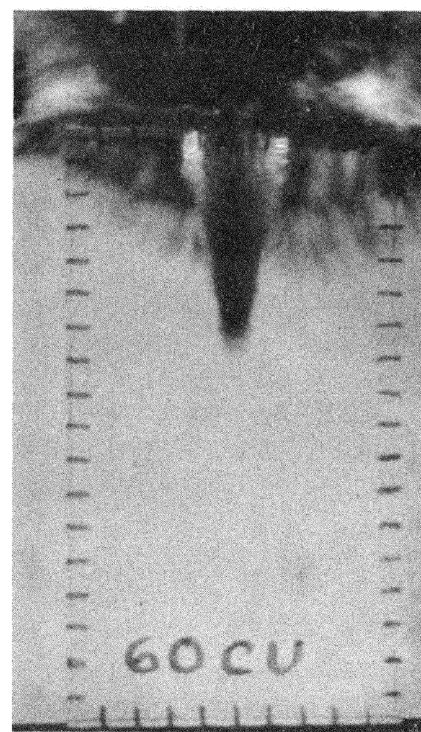
3 μ sec



12 μ sec



21 μ sec



30 μ sec

Figure 4. Penetration of 60° Copper JRC in Plexiglas

TABLE V
JET PENETRATION IN PLEXIGLAS

Shot Number	Liner Material	Liner Angle (deg)	Liner Diameter (cm)	Standoff (CD)	Penetration (CD)
1	Cu	100	1.27	1.25	4.12
5	Cu	100	1.27	1.25	5.35
14	Cu	100	1.27	1.25	4.72
15	Cu	100	1.27	1.25	4.88
16	Cu	100	1.27	1.25	5.00
18	Cu	100	1.27	1.25	4.88
21	Cu	100	1.27	1.25	5.26
22	Cu	100	1.27	1.25	4.76
23	Cu	100	1.27	1.25	4.00
24	Cu	100	1.27	1.25	4.50
25	Cu	100	1.27	1.25	5.75
2	Cu	60	1.27	1.25	6.00
3	Cu	60	1.27	1.25	4.62
4	Cu	60	1.27	1.25	5.9
6	Cu	60	1.27	1.25	6.08
19	Cu*	60	1.27	1.25	0.76
20	Cu	60	1.27	1.25	6.0
11	Al	100	1.27	1.25	2.6
7	Al	100	1.27	2.25	3.62
10	Al	80	1.27	1.25	3.02
9	Al	80	1.27	2.25	4.30
8	Ti	100	1.27	1.25	2.52
29	Al	60	1.59	2.00	5.31

*5Y Explosive used instead of RDX

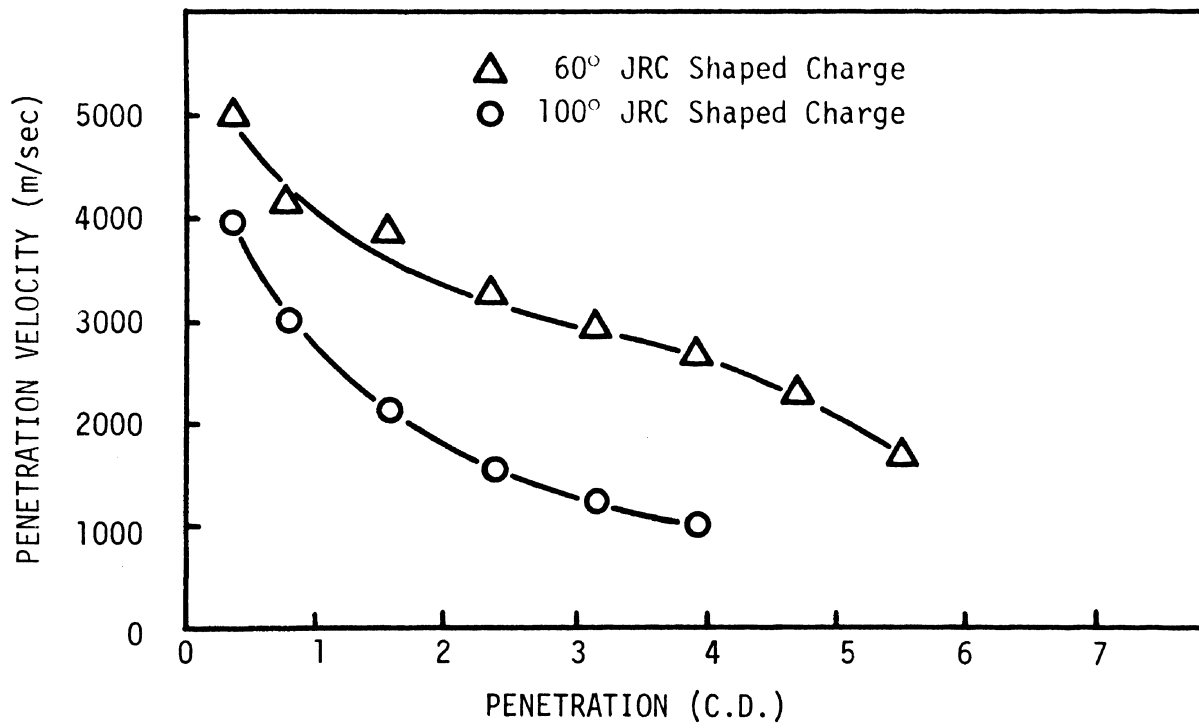


Figure 5. Penetration Velocity for 60° and 100° Copper JRC in Plexiglas

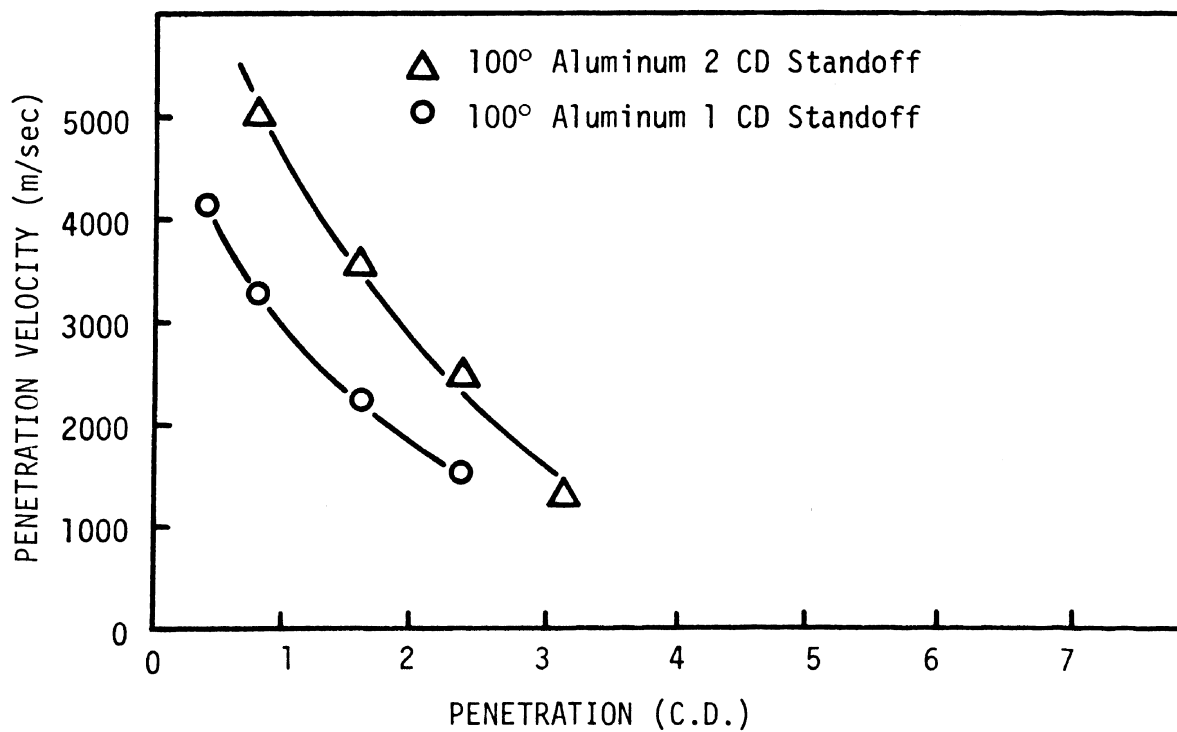


Figure 6. Penetration Velocity for 100° Aluminum JRC in Plexiglas

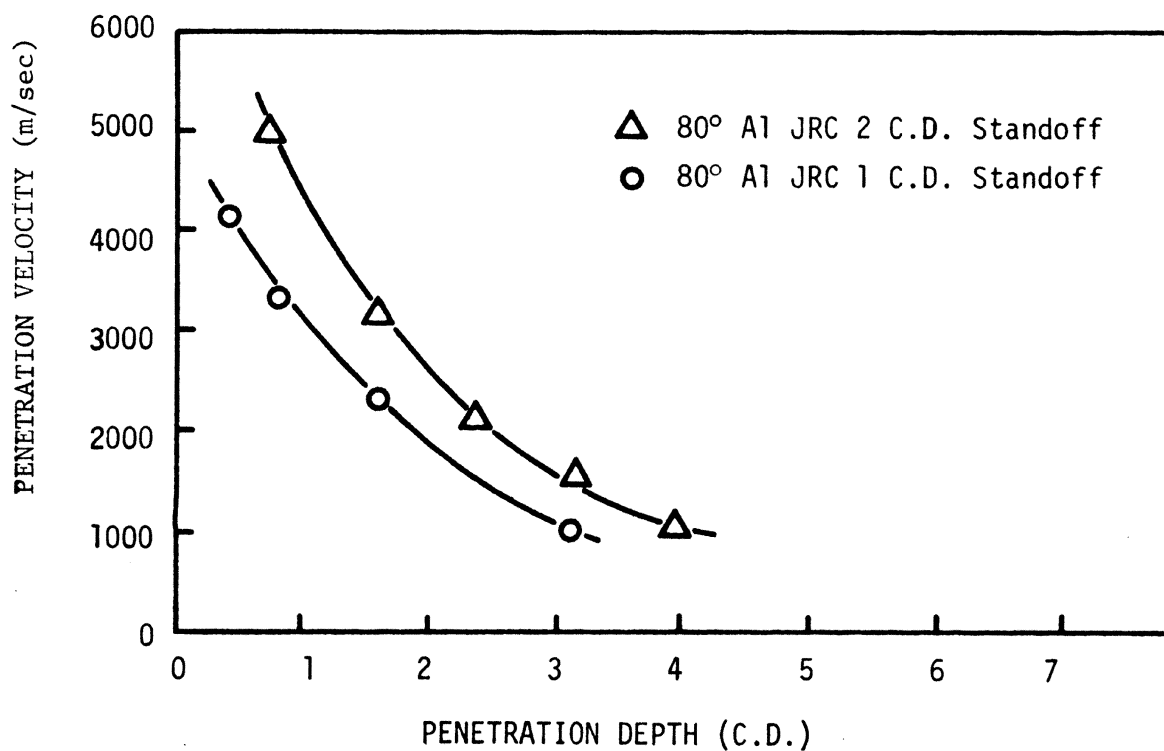


Figure 7. Penetration Velocity for 80° Aluminum JRC in Plexiglas

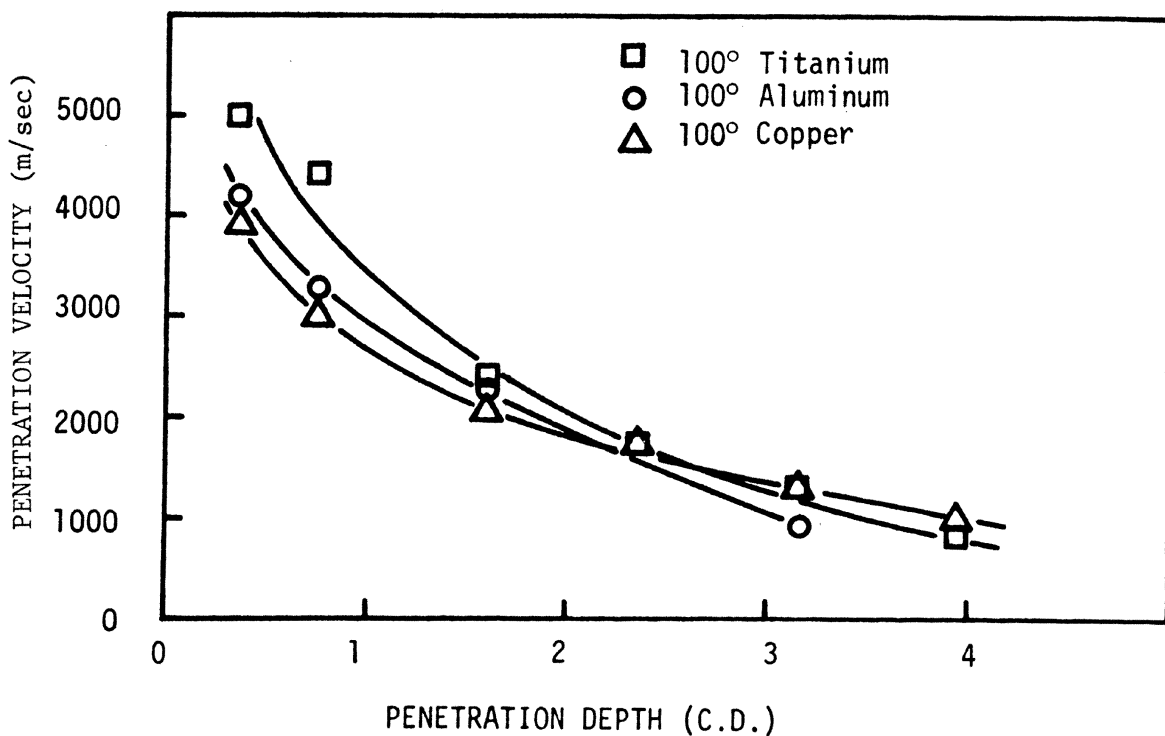
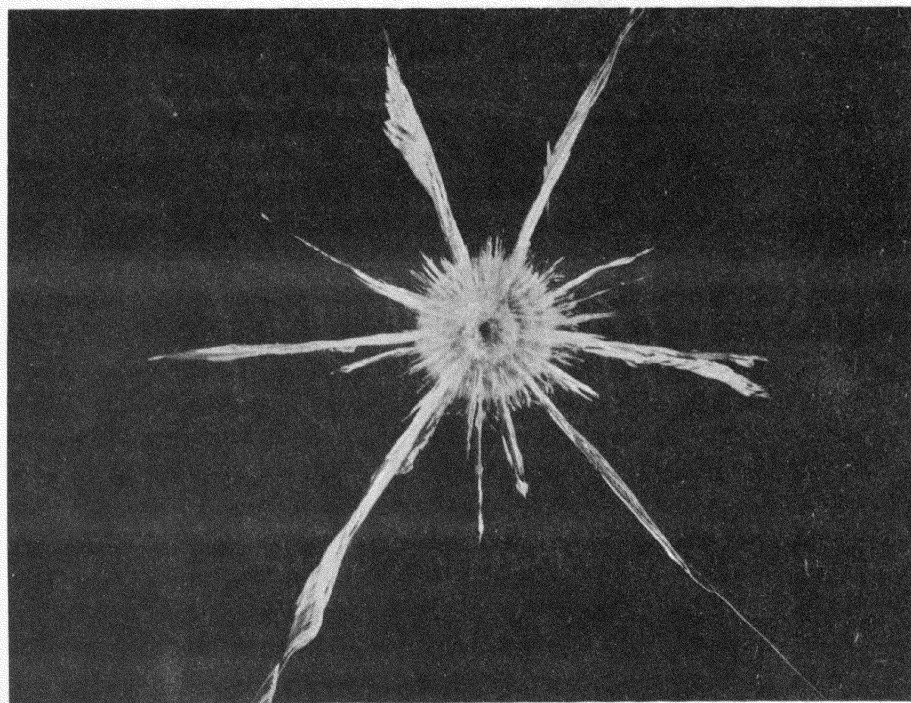
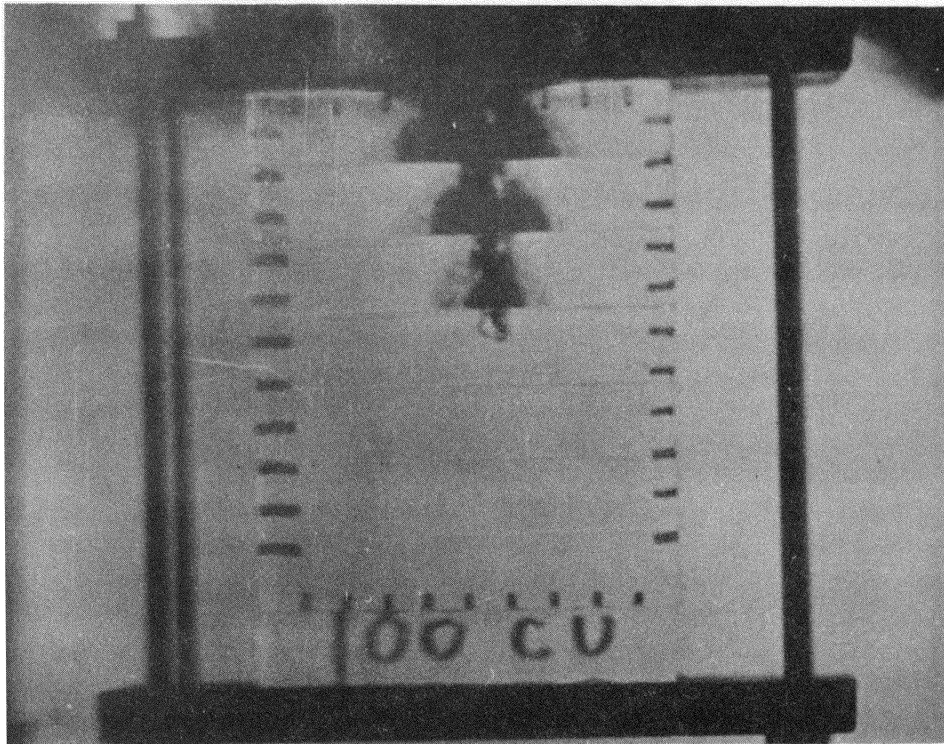


Figure 8. Penetration Velocity for 100° JRC in Plexiglas

and aluminum jets also evidenced the greatest decrease of velocity with penetration distance. The copper liner gave the deepest penetration of the three.

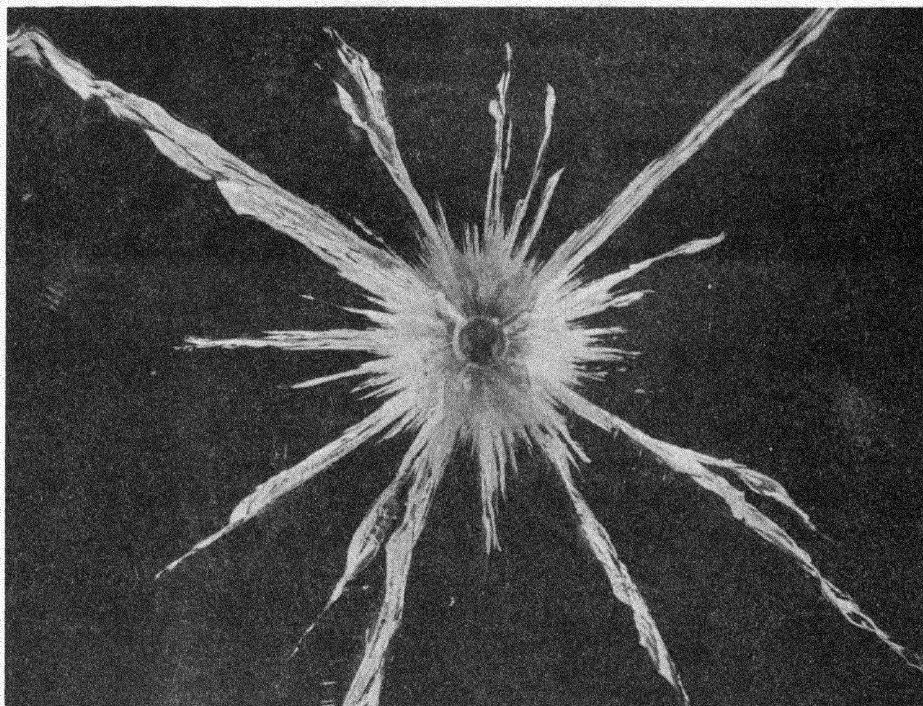
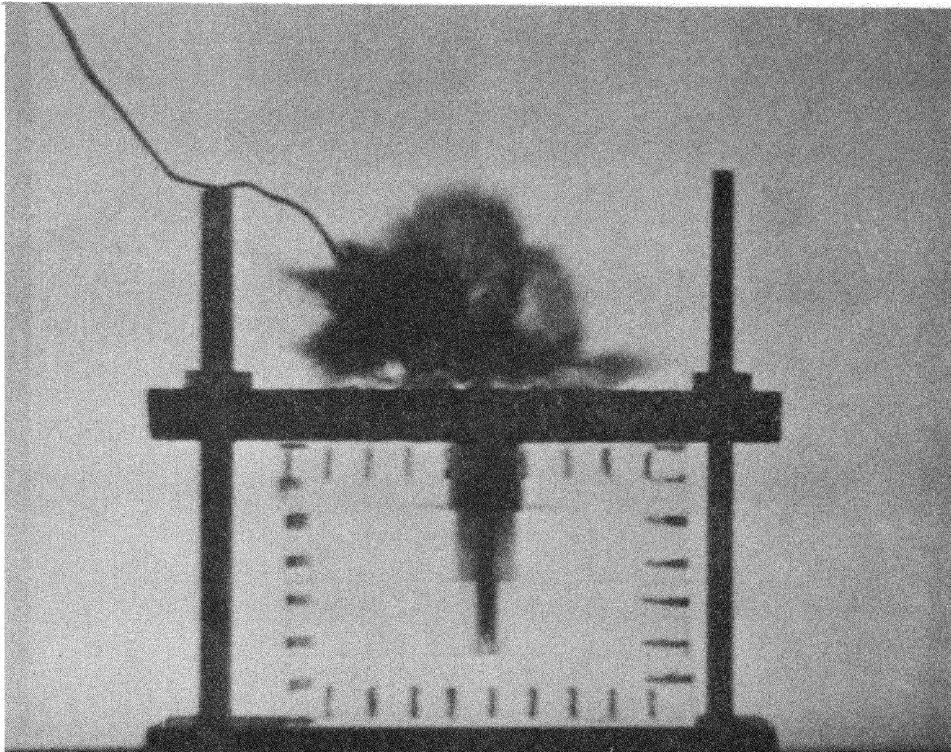
Plexiglas models constructed of 1.90 cm thick plates clamped together were used to simulate bedded models. Jets from shaped charges with 100° copper liners shot perpendicular to the bedding demonstrated a rapid decrease in velocity in relation to penetration distance. The fracture formation relative to the position along the jet length was no longer conical, in form, but approached a cylindrical limit with fracturing due to tensile reflections at the interfaces as an important breakage mechanism (Fig. 9). For comparison purposes a bedded Plexiglas model was drilled to a depth of 5.08 cm and loaded with 10 grain per foot mild detonating fuse (MDF) for the explosive charge. This model also showed that the conical form of fracture was modified by tensile reflections at the interface and the breakage was again cylindrical in outline (Fig. 10). Holes created by shaped charge jets fired parallel to the bedding exhibited penetration and fracture comparable to those in homogeneous models. However, fractures induced by the jet did not cross the bedding planes but were channeled between them (Fig. 11). A similar model was drilled and shot with 10 grain MDF, the fractures did not cross the bedding planes (Fig. 12).

A 100° copper lined charge was fired into a model at a 45° angle with the bedding and 2.5 CD standoff (Fig. 13). The initial penetration velocity was lower than that observed with similar charges at one CD standoff, but the rate of change of velocity with penetration depth was also less (Fig. 14). This indicates that in



Plan View of Second Layer

Figure 9. Jet Penetration Across Plexiglas Plates
(100° Copper JRC)



Plan View of Second Layer

Figure 10. 10 Grain MDF Across Plexiglas Plates

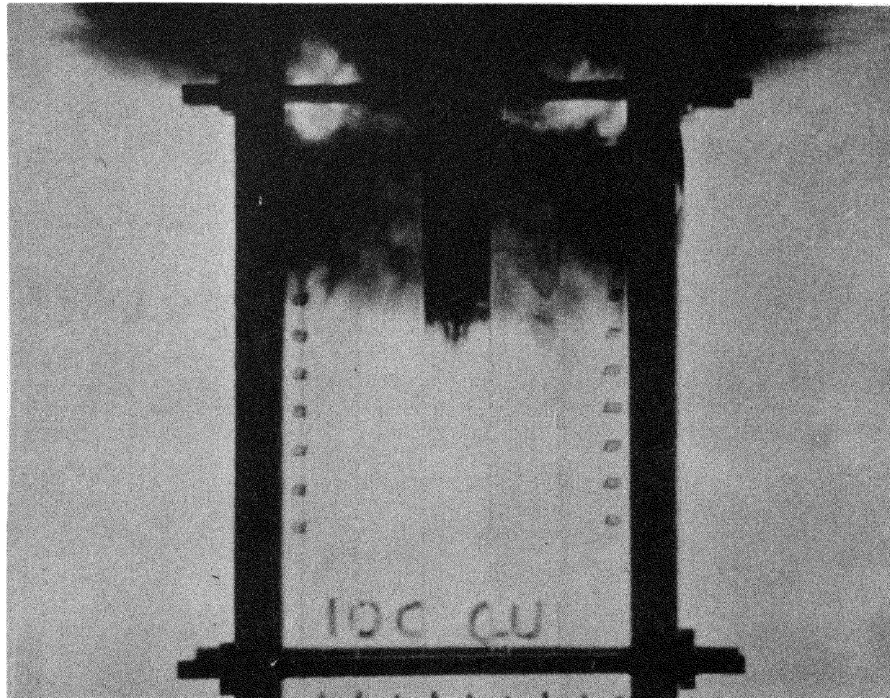


Figure 11. Jet Penetration Parallel to Plexiglas Plates (100° Copper JRC)

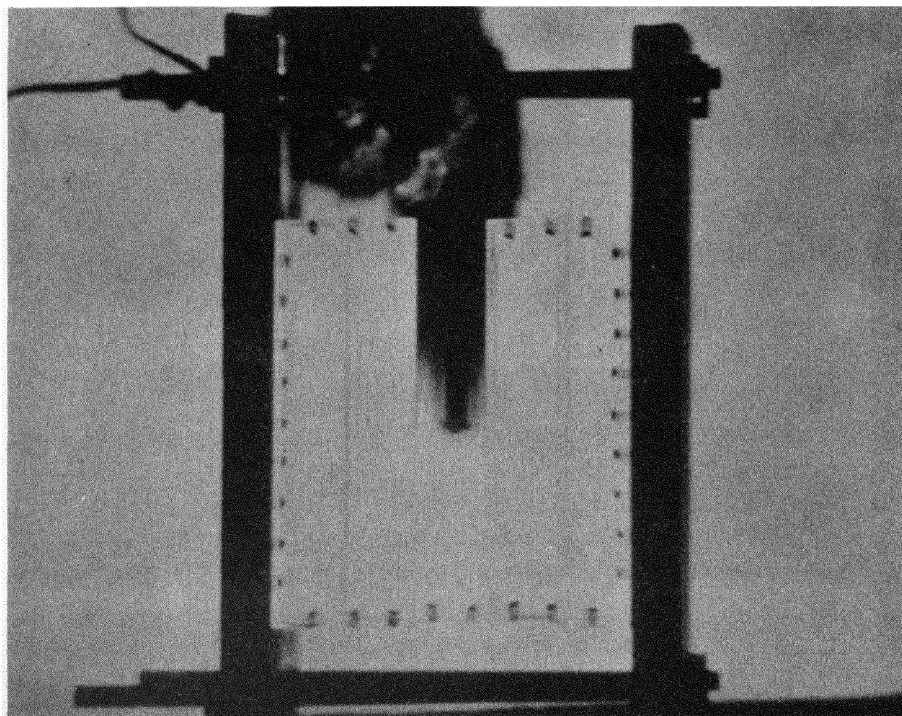


Figure 12. 10 Grain MDF Parallel to Plexiglas Plates

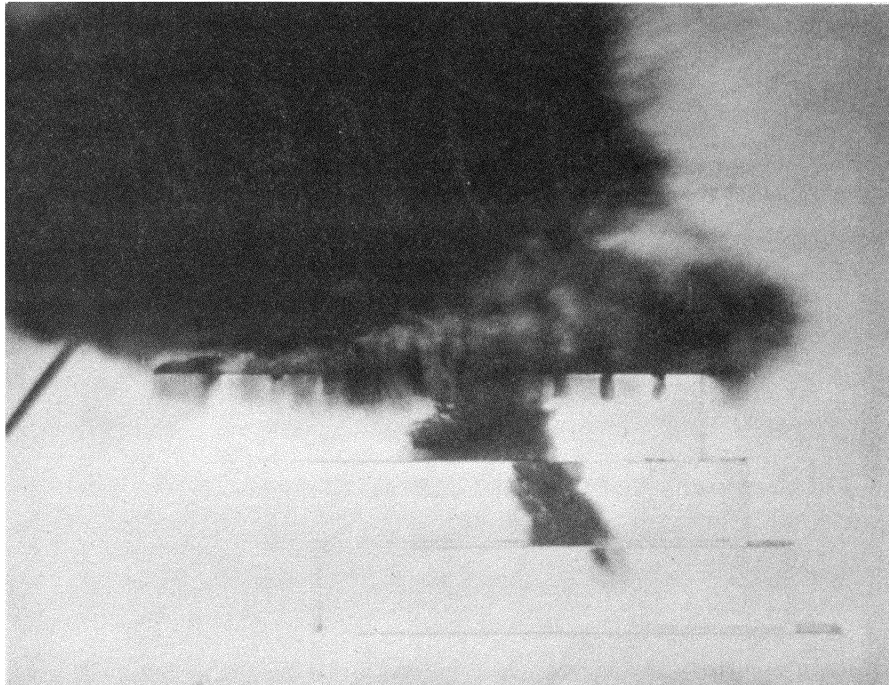


Figure 13. Jet Penetration for 100° Copper JRC
at 45° to Plexiglas Plates

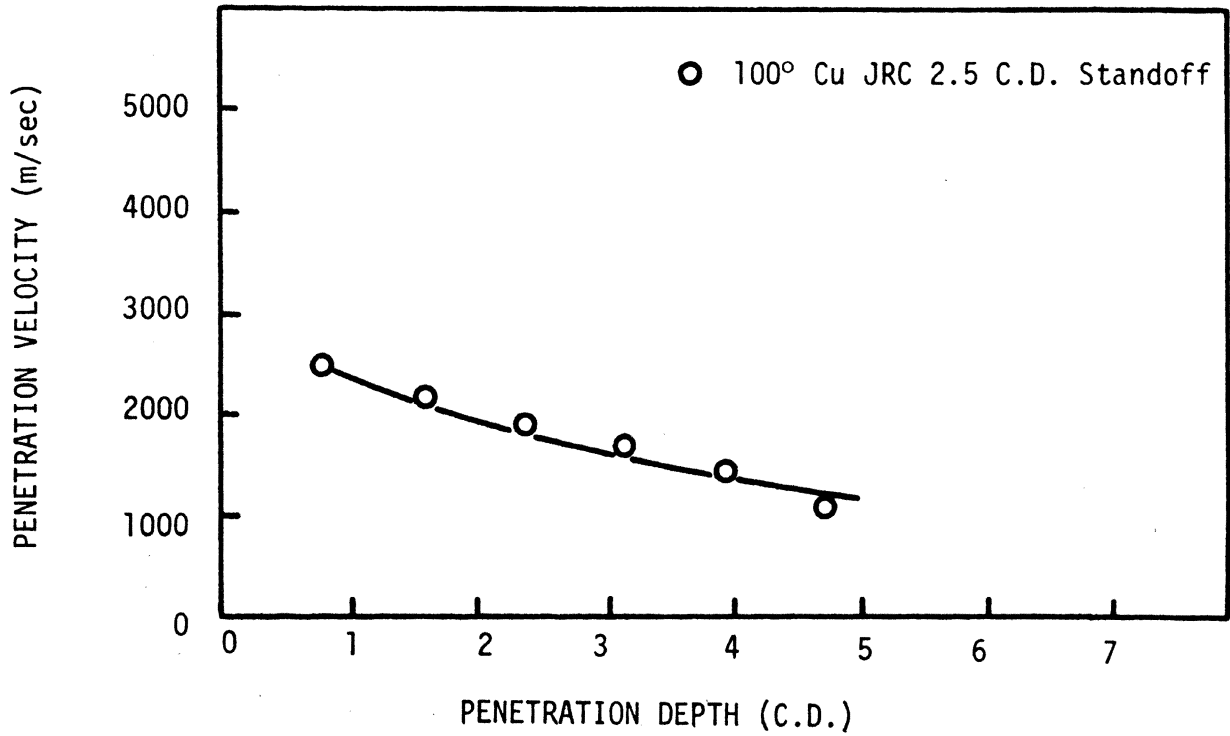


Figure 14. Penetration Velocity at 45° to Plexiglas Plates

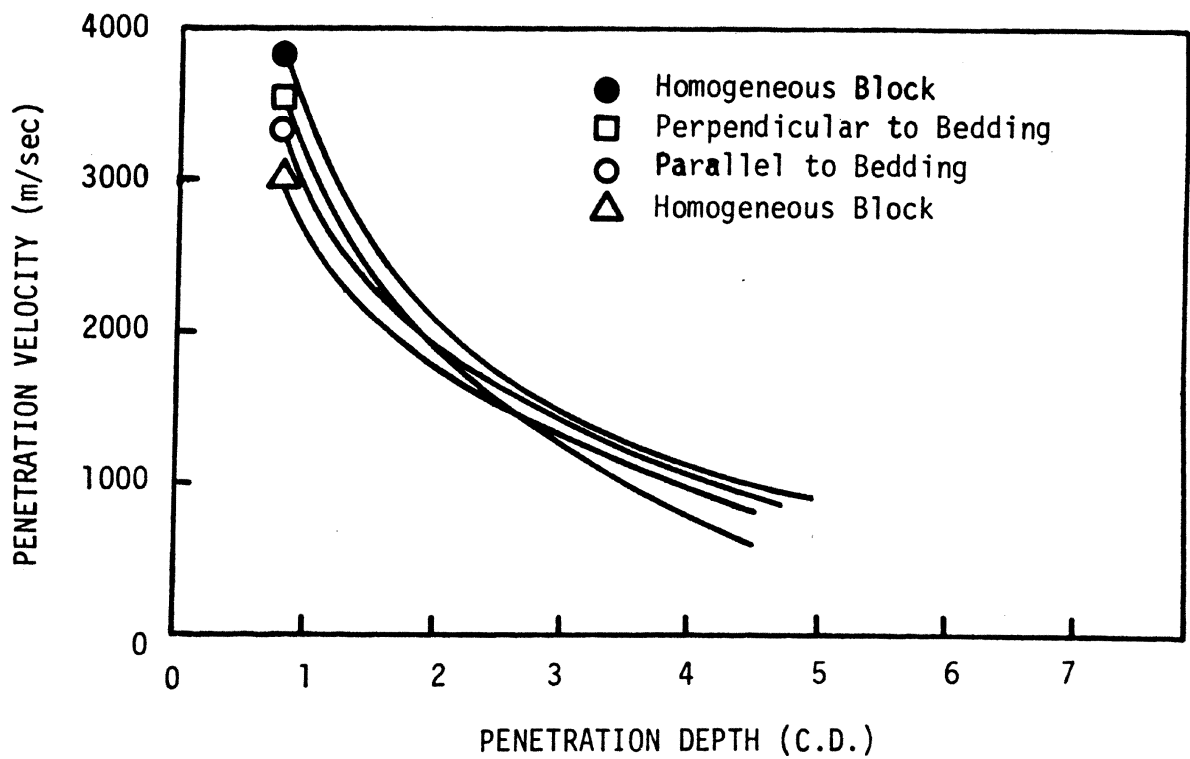


Figure 15. Penetration Velocity for 100° Copper JRC Liners in Plexiglas

accordance with theory there is an optimum standoff that maximizes continuous jet formation before it strikes the target.

A comparison was made of penetration and associated phenomena caused by charges with 100° copper liners fired at one CD standoff into homogeneous and bedded material. Penetration velocities over a given distance were approximately the same for two charges fired into homogeneous samples and for one shot parallel to the bedding (Fig. 15), while the velocity of the jet penetrating perpendicular to the bedding decreased more rapidly indicating energy loss at the interface. A 100° JRC fired at one CD standoff along the plane of the interface between two tightly clamped Plexiglas blocks resulted in fractures immediately around the hole but no large fractures were formed in either block (Fig. 16).

2. Dolomite

Charges with liner diameters of 4.76 cm were hand loaded with composition C4 and Gelcoalite Z, a permissible explosive, for tests in dolomite (Table VI). Liners with apex angles of 30° and 80° were machined from brass and aluminum with liner thicknesses scaled from the 1.27 cm diameter JRC charges (Table VII). The standoff for charges with brass liners was one CD while that for aluminum was 3 CD. A comparison of the penetration depth which resulted from the 30° and 80° brass lined charges loaded with composition C4 revealed that the maximum average penetration of 6.84 CD resulted from charges with 80° apex angles. The 80° brass liners also functioned best for charges loaded with Gelcoalite Z and demonstrated a penetration capability of 2.3 CD.

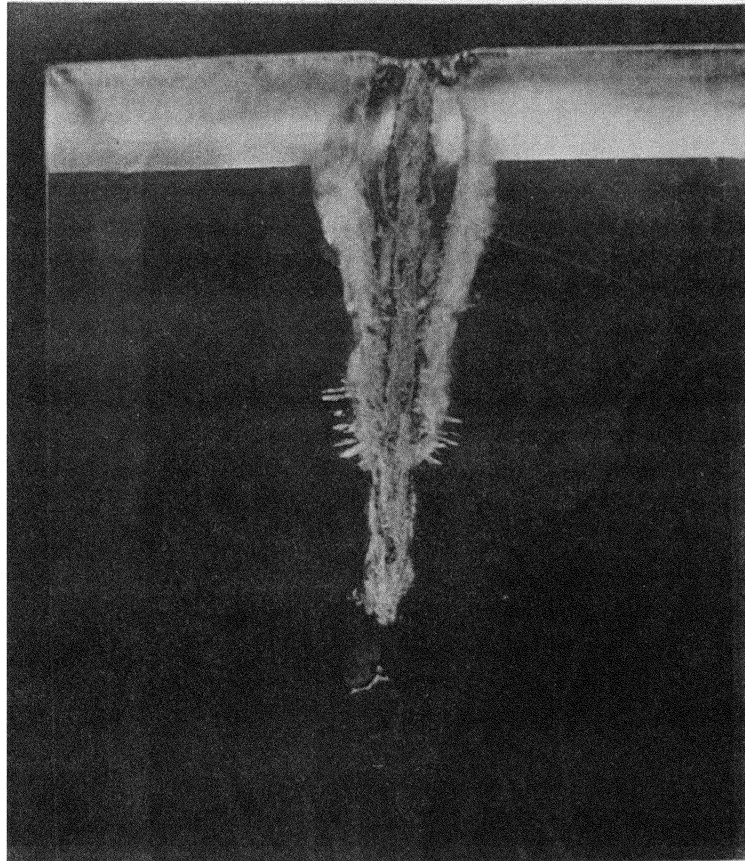


Figure 16. Jet Penetration Profile in Plexiglas

TABLE VI

JET PENETRATION IN DOLOMITE FOR 4.76 CM DIAMETER CHARGES

Liner Material	Liner Angle (deg)	Liner Thickness (mm)	Explosive	Standoff (CD)	Penetration (CD)
Al	80	3.8	Gelcoalite Z	3	1.73
Al	80	3.8	Gelcoalite Z	3	2.13
Al	80	3.8	Gelcoalite Z	3	1.87
Al	30	3.8	Gelcoalite Z	3	1.06
Al	30	3.8	Gelcoalite Z	3	1.16
Al	30	3.8	Gelcoalite Z	3	1.06
Al	80	3.8	C4	3	4.33
Al	80	3.8	C4	3	5.4
Al	80	3.8	C4	3	5.86
Al	80	3.8	C4	3	5.6
Al	80	3.8	C4	3	4.8
Al	80	3.8	C4	3	4.4
Al	80	3.8	C4	3	4.8
Brass	80	1.9	C4	1	8.0
Brass	80	1.9	C4	1	6.4
Brass	80	1.9	C4	1	6.13
Brass	80	1.9	Gelcoalite Z	1	2.67
Brass	80	1.9	Gelcoalite Z	1	2.13
Brass	80	1.9	Gelcoalite Z	1	2.20
80° angle cavity (no liner)			C4	1	

TABLE VII
JET PENETRATION IN GRANITE, DOLOMITE AND COAL

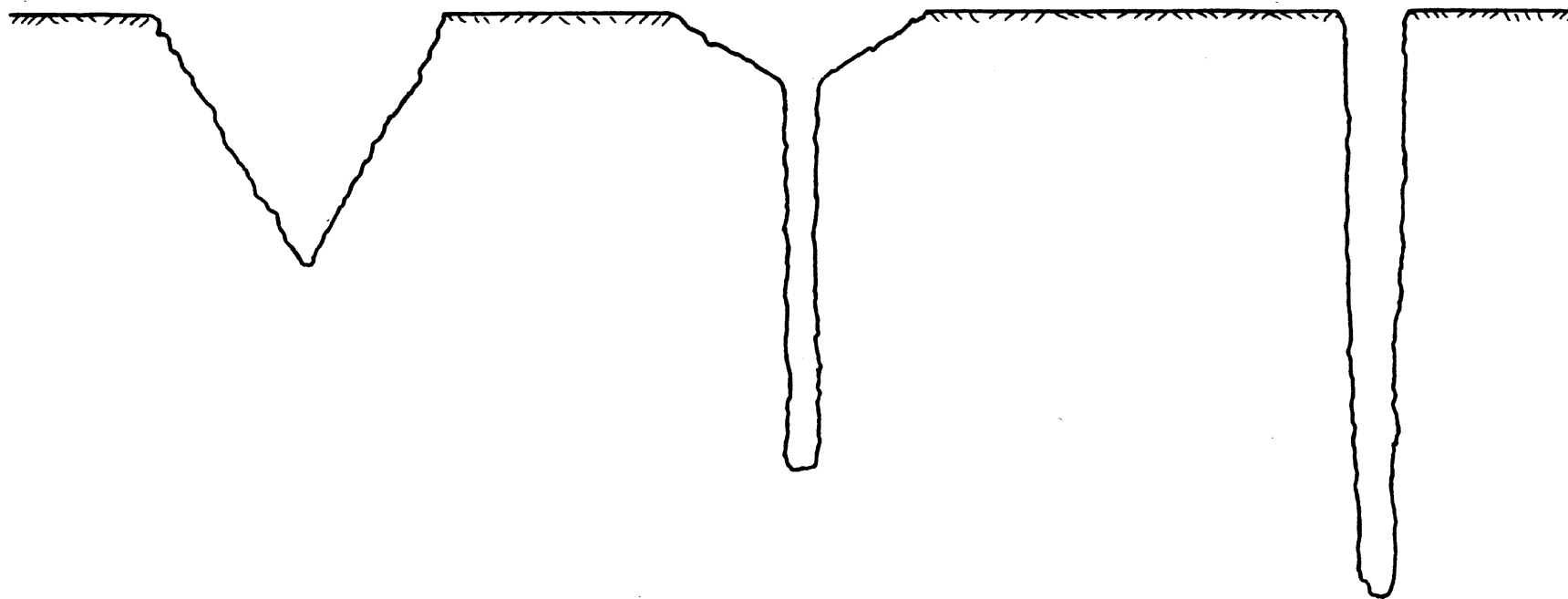
<u>Liner Material</u>	<u>Liner Angle (deg)</u>	<u>Liner Diameter (cm)</u>	<u>Liner Thickness (cm)</u>	<u>Explosive</u>	<u>Standoff (CD)</u>	<u>Penetration (CD)</u>	<u>Rock Type</u>	<u>Bedding Orientation</u>
Cu	55	2.06	0.076	RDX	2.2	2.61	Granite	
Cu	100	3.30	0.102	RDX	2.3	3.07	Granite	
Cu	55	2.06	0.076	RDX	2.2	3.99	Dolomite	
Cu	100	3.30	0.102	RDX	2.3	4.2	Dolomite	
Al	80	1.27	0.102	RDX	3.0	3.5	Dolomite	
Al	80	1.27	0.102	RDX	3.0	3.0	Dolomite	
Al	80	1.27	0.102	RDX	3.0	3.75	Dolomite	
Brass	60	1.59	0.102	C4	0.8	6.8	Coal	parallel
Brass	60	1.59	0.102	C4	0.8	7.6	Coal	parallel
Cu	55	2.06	0.076	RDX	2.2	9.84	Coal	parallel
Cu	55	2.06	0.076	RDX	0.6	7.68	Coal	parallel

Jet penetration depth was observed to be related to the depth of the surface crater formed when shaped charge jets penetrated dolomite (Fig. 17). This phenomenon was a result of the collapse mechanism of the liner. The mass, velocity gradient, and cross sectional area at any given point along the jet should remain constant for all charges of the same geometry. The detonation pressure, which is responsible for the liner collapse, is also constant for a given explosive. Non-uniform liner thickness or other geometric conditions which deviate from the ideal can cause particles extruded into the jet by the collapsing cone to deviate from the coherent jet cross section formed under ideal conditions. This deviation results in a shorter continuous jet with reduced penetration capabilities. The particles which strike the rock surface incoherently are responsible for the surface spall (Fig. 18). A charge was constructed with an unlined 80° cavity and composition C4 as the explosive and fired with no standoff. The resulting flat bottomed crater was 12.7 cm in diameter and 2.54 cm deep.

Three 1.27 cm (0.5 in.) JRC charges with 80° aluminum liners were also fired into dolomite resulting in an average penetration of 3.42 CD. The calculated scaled penetration for the 4.76 cm diameter liners with scaled dimensions was 3.42 CD but the measured value was 5.06 CD for an abnormal scaling factor of 1.48 between these two charge diameters.

3. Coal

Jet penetration from JRC charges in dolomite and Plexiglas produced holes with linear sides and uniform taper. The hole profiles



Surface Crater

Surface Crater and Hole
Formed by Jet

Hole Formed by Jet
with no Surface Crater

Figure 17. CRATER PROFILES IN DOLOMITE

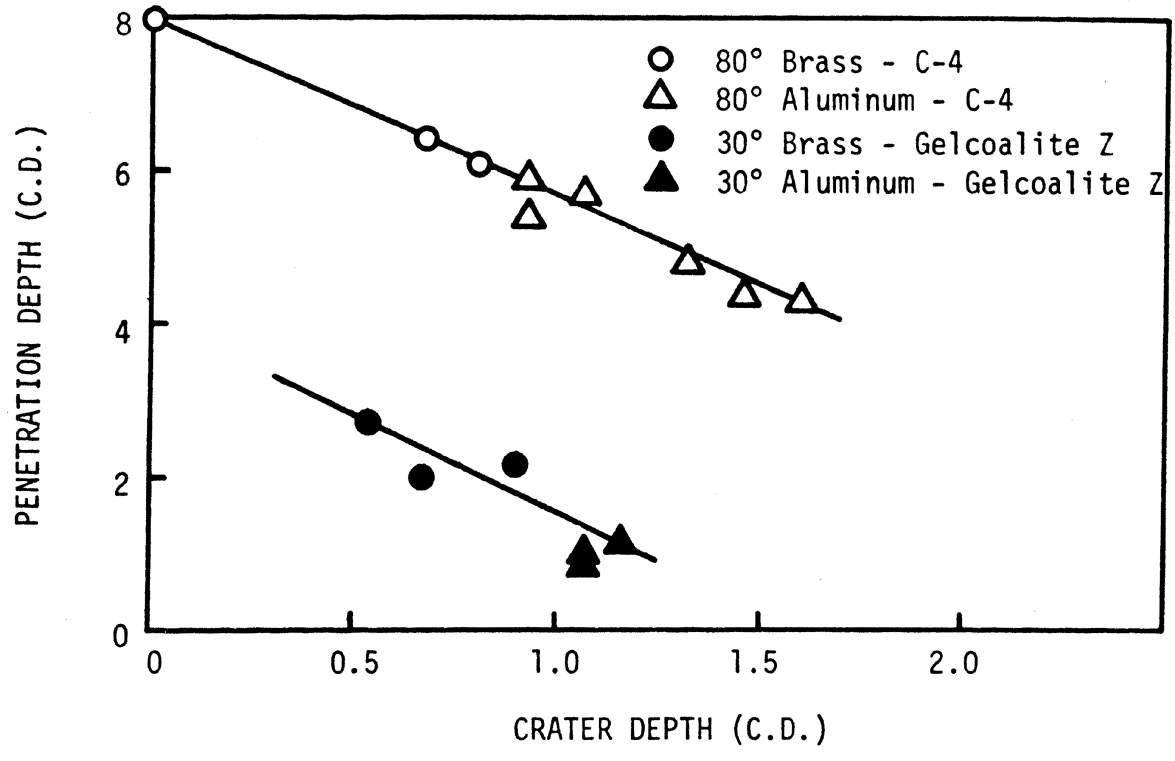


Figure 18. Jet Penetration and Crater Depths in Dolomite

in coal showed differences in diameter which were related to the type of material between the particular bedding planes. Jet penetration in dolomite and Plexiglas resulted in a slightly tapering straight hole while the hole axis in coal did not always follow a straight line and some deviation was observed (Fig. 19). This indicates that liner imperfections and jet formation influence the target response in terms of the size and direction of the final hole produced after the pressure and stress are relieved.

Penetration and fracture data were obtained from the large samples used for the permeability study (Tables III and IV). Jets from charges with copper liners and 60° apex angles penetrated to almost 11 CD while all other liners tested gave values between 7 and 8 CD, except for the 80° aluminum liner utilizing a standoff of only 0.25 CD. The jet from this liner penetrated only 3.26 CD, forming a crater, and no characteristic hole was observed (Table VIII). Jet penetration effectiveness was less for 60° copper liners when the standoff was reduced to 0.25 CD (Fig. 20). Results from experiments with Plexiglas indicated that penetration velocity was slower when the jet crossed bedding planes in laminated models than that observed in homogeneous samples. The average penetration in coal decreased by 8 percent when charges were fired perpendicular to the bedding planes.

Radiographs were taken as jets from JRC, 60° copper liners penetrated coal specimens (Fig. 21). The jet penetration velocity was affected when the standoff was changed from 1.25 CD to 0.25 CD (Fig. 22). At the larger standoff the initial penetration velocity was greater than at 0.25 CD standoff. At a penetration depth of

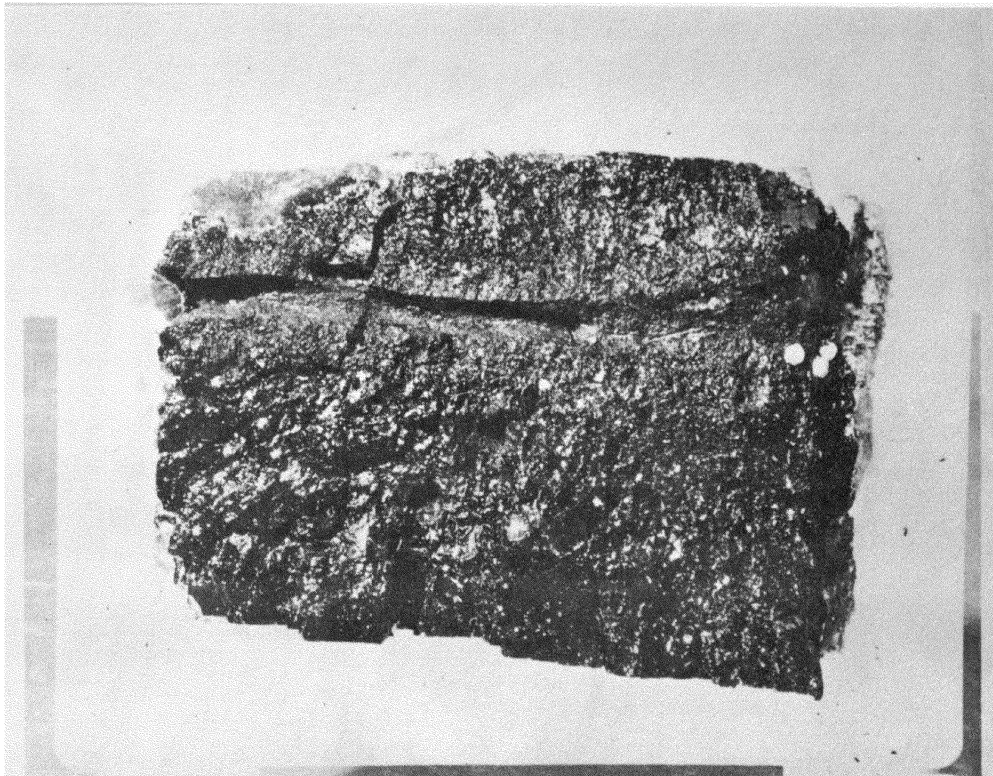


Figure 19. Jet Profile in Coal

TABLE VIII
AVERAGE PENETRATION IN COAL BY JRC CHARGES

<u>Liner Material</u>	<u>Liner Angle (deg)</u>	<u>Standoff (CD)</u>	<u>Penetration Parallel (CD)</u>	<u>Penetration Perpendicular (CD)</u>
Cu	100	1.25	8.16	6.92
Cu	60	1.25	11.00	10.55
Al	100	2.25	7.78	7.15
Al	80	2.25	7.70	7.75
Cu	60	0.25	9.33	--
Al	80	0.25	3.36	--

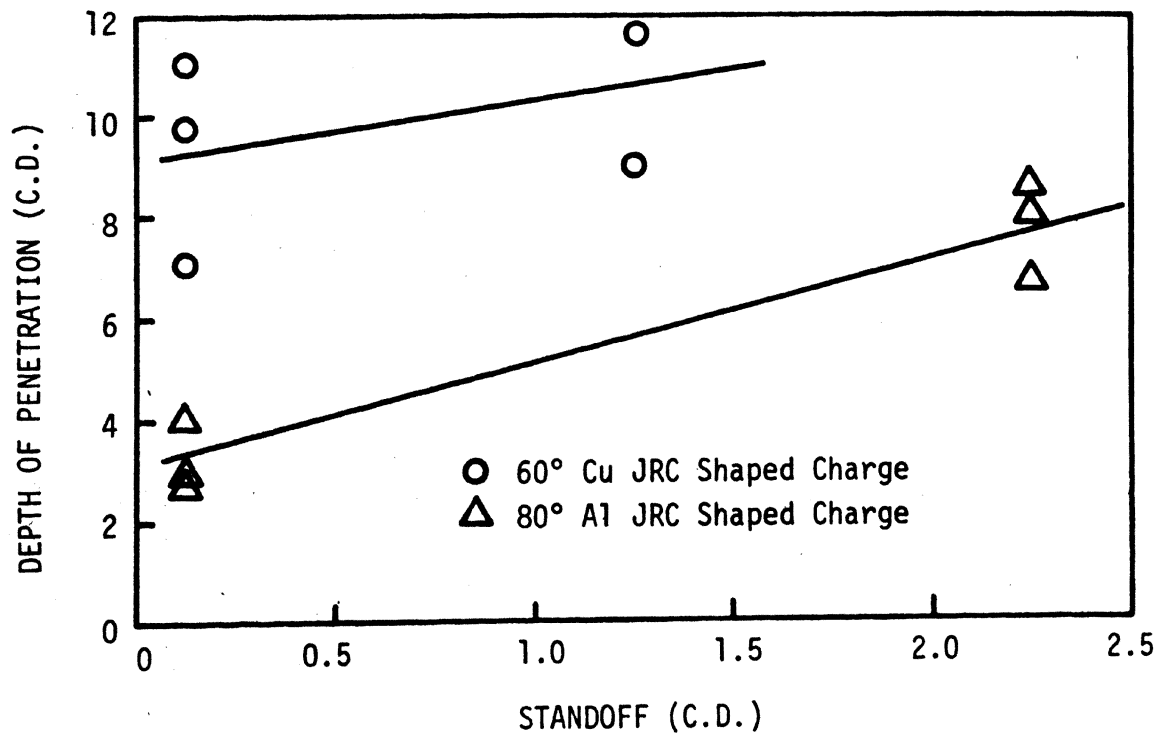


Figure 20. Penetration Depth Vs Standoff Distance in Coal

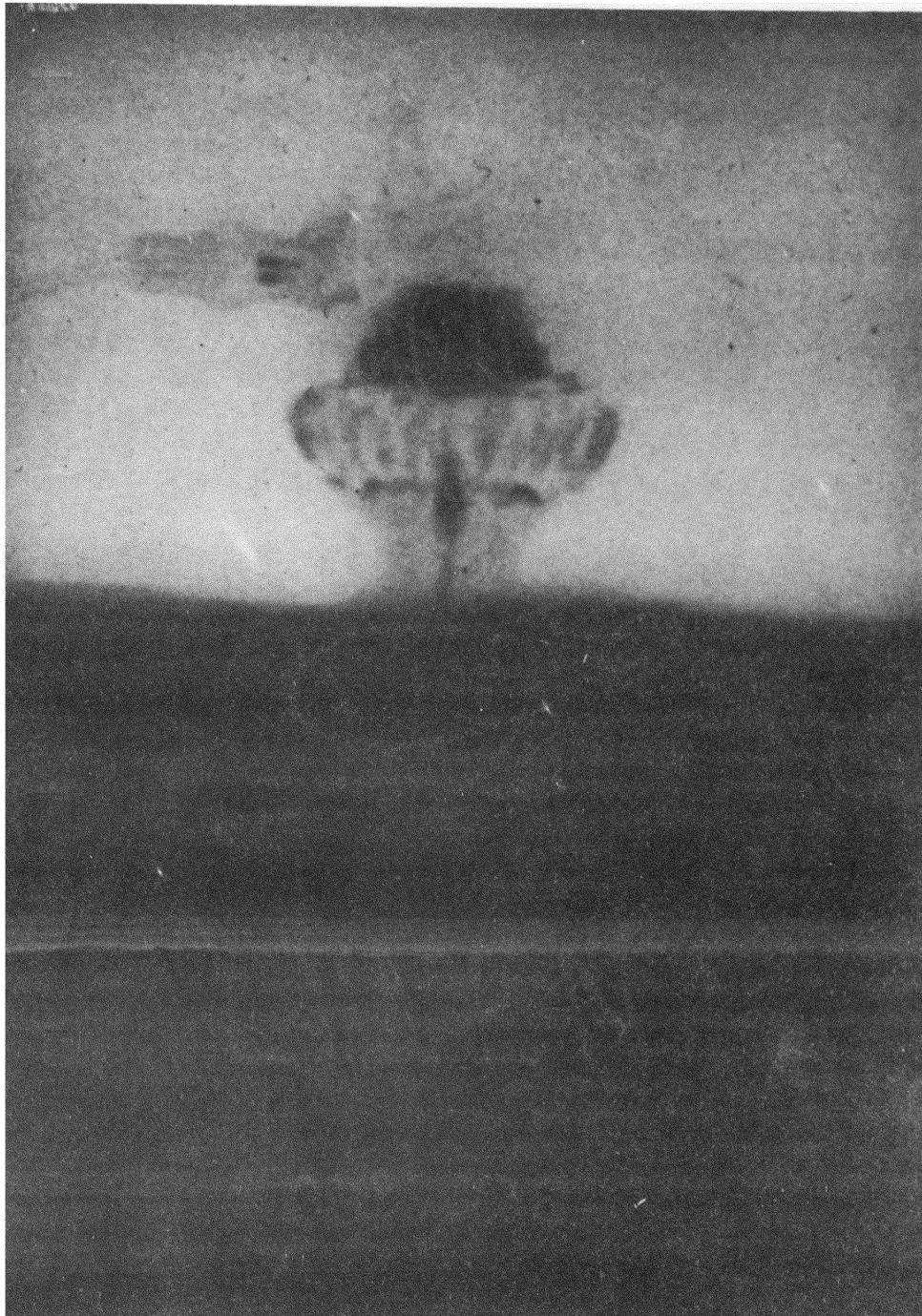


Figure 21. Radiograph of 60° Copper JRC in Coal

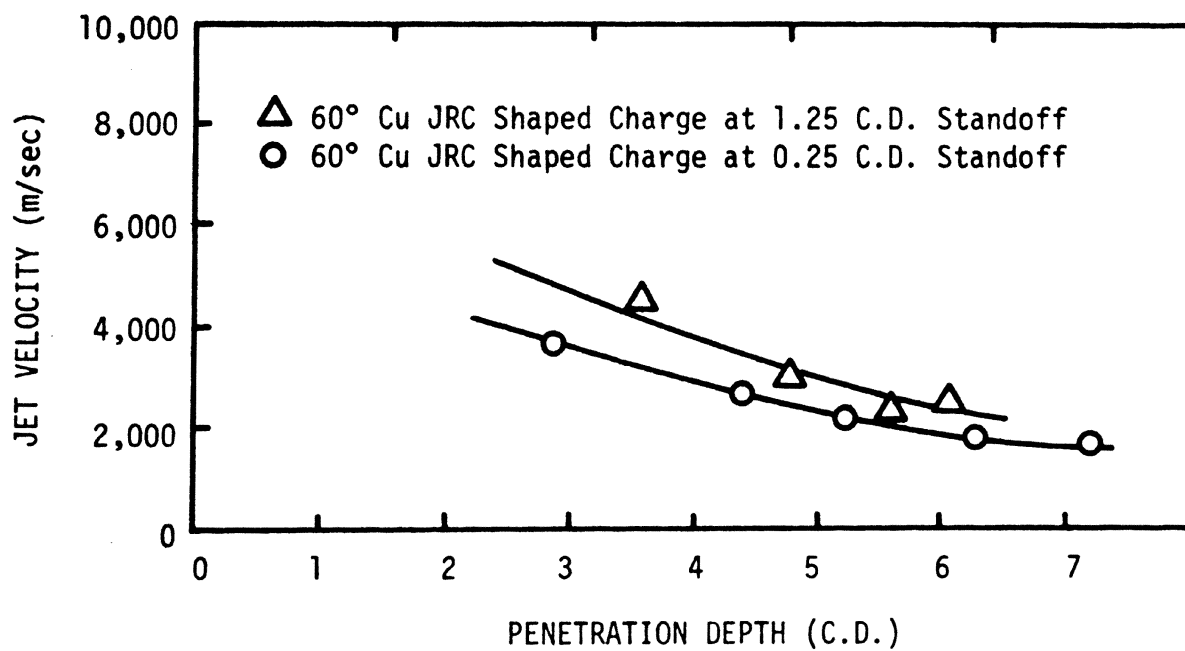


Figure 22. Jet Penetration Velocity in Coal

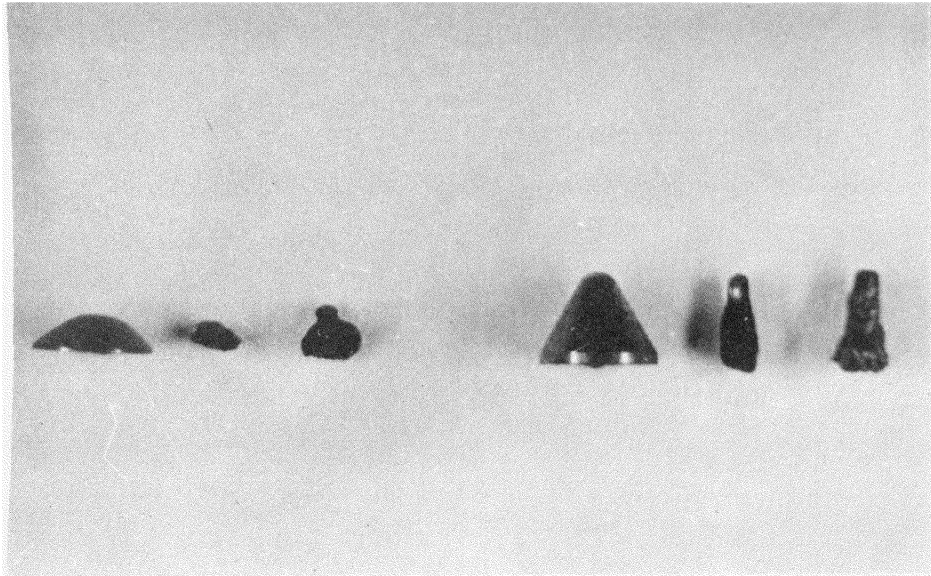
4 cm the velocity of the jet in coal was 50 percent greater than that observed in Plexiglas. A particulate jet was observed 40 μ sec after initiation of the charge. The slug velocity was calculated from radiographs to be 500 meters per second.

Shaped charges with permissible explosives were used to determine the effect of detonation velocity on jet penetration in coal. Charges loaded with Atlas 5Y, having a velocity of 1800 meters per second, formed weak, incomplete jets. Maximum penetration resulted from charges with 60° copper liners (Table IX) and slugs were recovered from all liner materials. The 60° copper liners collapsed towards the cone axis while the aluminum liners behaved more like projectiles (Fig. 23). The 100° titanium liners turned inside out, and the central portion of the liner was destroyed. The collapse process of the 100° copper liner differed from that of the titanium in that a frozen jet was formed (Fig. 23) indicating partial liner collapse.

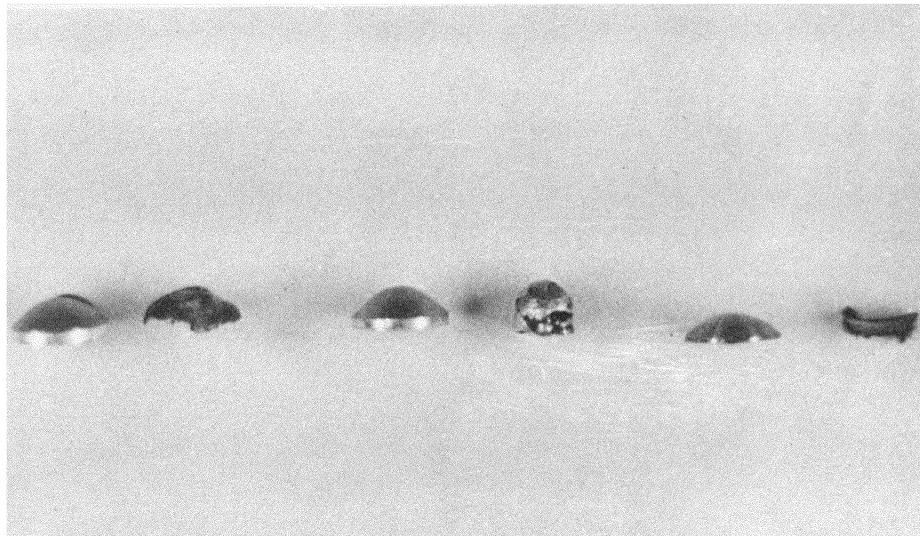
Charges were also prepared with the other two permissible explosives: Atlas 5U, velocity 2600 meters per second, and Atlas Gelcoalite Z, velocity 4300 meters per second. The results from these two explosives were similar to those obtained with Atlas 5Y, the difference being that the penetration was greater (Tables X and XI). The copper liners formed coherent jets and deformed, while liners of other metals impacted into the coal acting as projectiles. DuPont 40 percent special gelatin was loaded in charges with 60° copper and 80° aluminum liners. The velocity of this explosive is comparable to that of Gelcoalite Z, but no jet formation was observed (Table XII).

TABLE IX
PENETRATION - ATLAS 5Y

Shot Number	Liner Material	Liner Angle (deg)	Liner Diameter (cm)	Standoff (CD)	Penetration (CD)
5Y-1	Cu	100	1.27	1.25	1.25
5Y-2	Cu	100	1.27	1.25	1.12
5Y-3	Cu	100	1.27	1.25	1.12
5Y-4	Cu	100	1.27	3.00	1.25
5Y-5	Cu	100	1.27	1.25	1.25
5Y-6	Cu	60	1.27	1.25	2.25
5Y-7	Cu	60	1.27	1.25	1.25
5Y-8	Cu	60	1.27	1.25	2.38
5Y-9	Cu	60	1.27	1.25	2.13
5Y-10	Al	100	1.27	1.25	.75
5Y-11	Al	100	1.27	1.25	.75
5Y-12	Al	100	1.27	3.00	1.12
5Y-13	Al	80	1.27	3.00	1.50
5Y-14	Al	80	1.27	1.25	2.50
5Y-15	Al	80	1.27	1.25	1.75
5Y-16	Al	80	1.27	1.25	1.00
5Y-17	Ti	100	1.27	1.25	1.50



From Left: 100° Copper Liner, Slug using RDX, Slug using Coalite 5Y; 60° Copper Liner, Slug using RDX, Slug using Coalite 5Y



From Left: 100° Aluminum Liner, Slug using Coalite 5Y; 80° Aluminum Liner, Slug using Coalite 5Y; 100° Titanium Liner, Slug (inside out liner) using Coalite 5Y

Figure 23. Slugs from Shaped Charge Liners

TABLE X
PENETRATION - ATLAS 5U

<u>Shot Number</u>	<u>Liner Material</u>	<u>Liner Angle (deg)</u>	<u>Liner Diameter (cm)</u>	<u>Standoff (CD)</u>	<u>Penetration (CD)</u>
5U-1	Cu	60	1.27	1.25	3.25
5U-2	Cu	60	1.27	1.25	1.75
5U-3	Cu	60	1.27	1.25	2.00
5U-4	Al	80	1.27	1.25	1.35
5U-5	Al	80	1.27	1.25	1.75
5U-6	Al	80	1.27	1.25	1.35

TABLE XI
 PENETRATION - ATLAS GELCOALITE Z

<u>Shot Number</u>	<u>Liner Material</u>	<u>Liner Angle (deg)</u>	<u>Liner Diameter (cm)</u>	<u>Standoff (CD)</u>	<u>Penetration (CD)</u>
Z-1	Cu	100	1.27	1.00	3.00
Z-2	Cu	100	1.27	1.00	2.25
Z-3	Cu	100	1.27	1.00	2.00
Z-4	Cu	60	1.27	1.00	3.25
Z-5	Cu	60	1.27	1.00	3.00
Z-6	Cu	60	1.27	1.00	3.00
Z-7	Al	80	1.27	1.00	1.37
Z-8	Al	80	1.27	1.00	1.37
Z-9	Al	80	1.27	3.00	1.75
Z-10	Al	100	1.27	1.00	2.00
Z-11	Al	100	1.27	1.00	2.00
Z-12	Al	100	1.27	3.00	2.00

TABLE XII
PENETRATION - DUPONT 40% SPECIAL GELATIN

<u>Shot Number</u>	<u>Liner Material</u>	<u>Liner Angle (deg)</u>	<u>Liner Diameter (cm)</u>	<u>Standoff (CD)</u>	<u>Penetration (CD)</u>
SG-1	Cu	60	1.27	1.25	1.25
SG-2	Cu	60	1.27	1.25	1.00
SG-3	Al	80	1.27	1.25	1.00
SG-4	Al	80	1.27	1.25	.50
SG-5	unlined	80	1.27	1.25	1.50

Results of incomplete jet formation were observed in all charges using permissible dynamites and 60° copper liners. The inhomogeneity of the explosive caused many of the liners to collapse nonuniformly. The grain size of some of the explosives was large compared to the cone dimensions (1.27 cm diameter) resulting in nonuniform loading densities which affected the detonation velocity and liner collapse. The 4.76 cm diameter charges with brass liners loaded with Gelcoalite Z and fired into dolomite formed coherent jets, probably because the effect of the relative grain size was not as pronounced. Reducing the grain size of the permissible dynamite would give a more uniform loading density which would increase penetration for the 1.27 cm diameter charges.

4. Steel, Titanium and Lead

A series of tests was conducted in steel, titanium and lead to determine the jet penetration characteristics in non-brittle materials which exhibit hydrodynamic behavior when subjected to the pressure originating from a shaped charge jet (Table XIII).

The cavity cross section in titanium and steel was similar to that observed in coal, dolomite, and Plexiglas being cylindrical in form and tapered slightly toward the bottom. The cross section in lead, however, was of conical shape with radial dimensions 4 to 5 times greater than observed in the other materials tested.

C. Explosive Detonation Velocity

The studies conducted in dolomite suggest that jet penetration for geometrically similar charges at a given standoff is a function

TABLE XIII
PENETRATION DATA FOR METALLIC TARGETS

<u>Liner Material</u>	<u>Liner Angle (deg)</u>	<u>Target Material</u>	<u>Penetration (cm) (CD)</u>		<u>Diameter at Entry (cm)</u>
Cu	100	Steel	1.54	1.21	0.62
Cu	60	Steel	3.50	2.75	0.50
Cu	60	Steel	2.15	1.69	0.50
Cu	60	Steel	3.81	3.00	-
Cu	60	Ti	3.50	2.75	0.43
Cu	60	Ti	3.56	2.80	0.36
Cu	100	Ti	2.03	1.60	0.36
Cu	60	Pb	6.60	5.20	2.09
Cu	60	Pb	6.42	5.06	2.10

of the detonation velocity squared (Fig. 24). Data obtained from 1.27 cm diameter charges with 60° and 100° copper liners fired into coal also follow the same trend (Figs. 25 and 26).

D. Jet Tip Velocity

The pin oscillograph technique was employed to determine the velocity in air of the jet from a 60° copper JRC charge (Fig. 27). The velocity decreased to approximately 5000 meters/second after traveling about 10 cm from the charge and maintained this velocity for the next 12 cm.

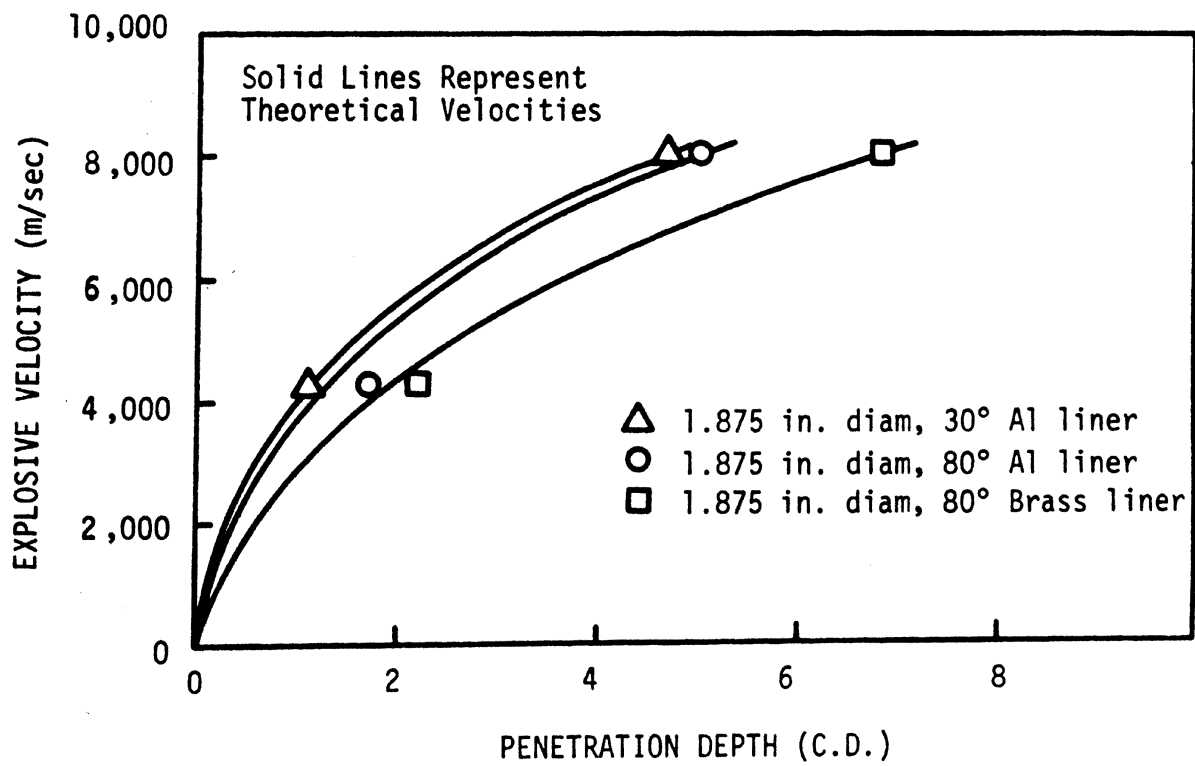


Figure 24. Penetration in Dolomite

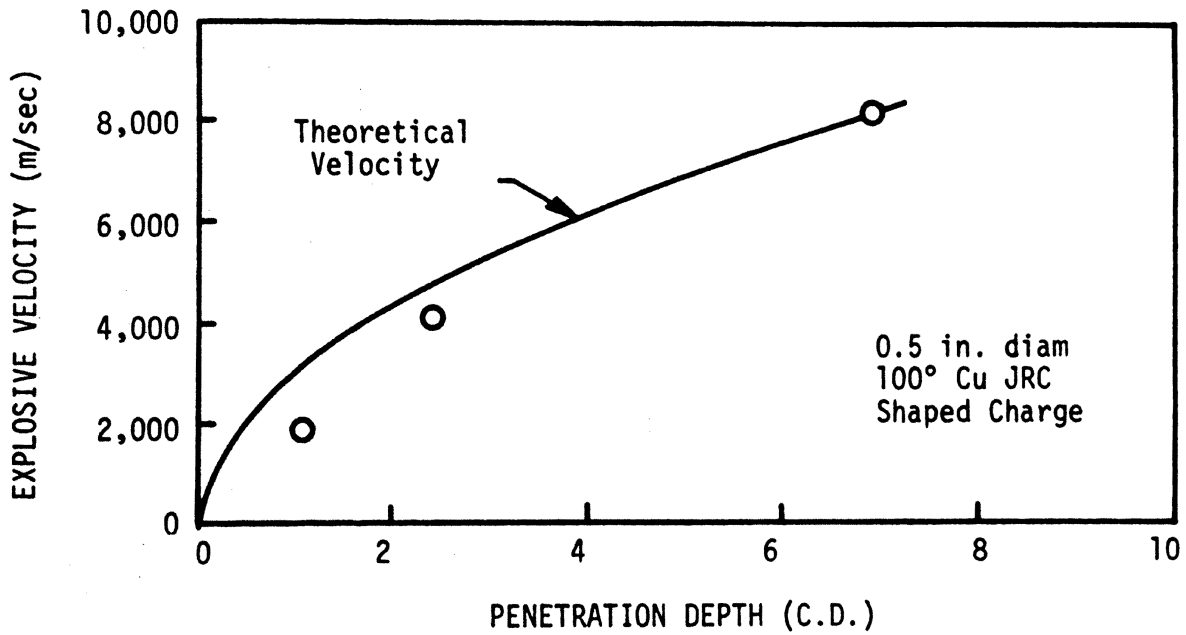


Figure 25. Penetration Depth Perpendicular to Coal Bedding (100° Copper JRC)

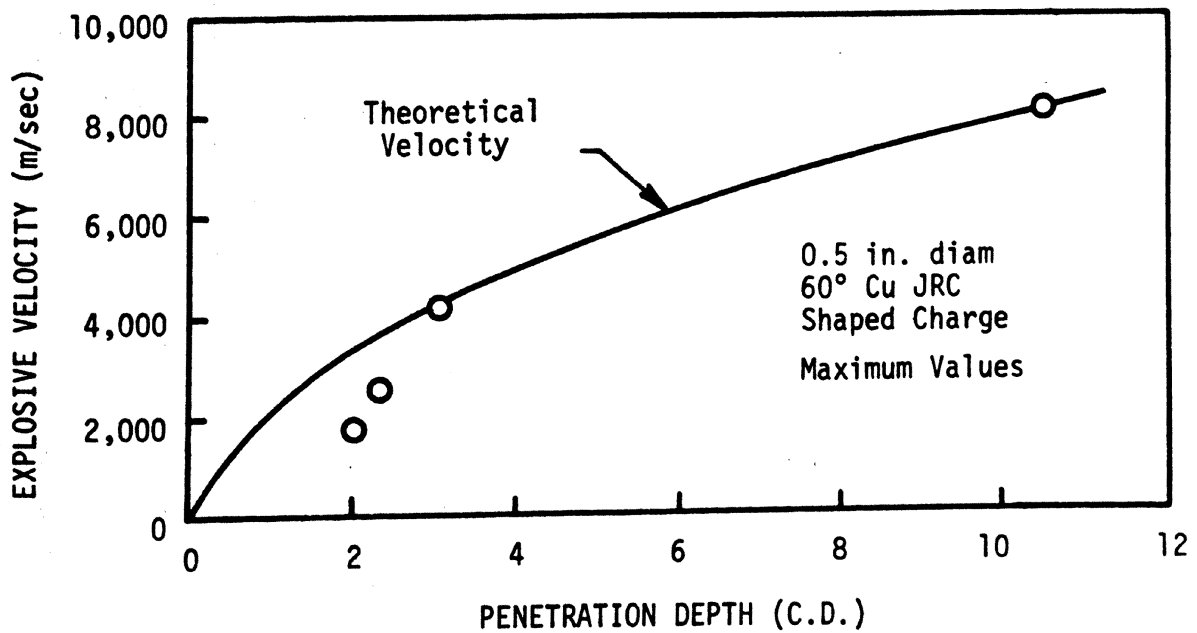


Figure 26. Penetration Depth Perpendicular to Coal Bedding (60° Copper JRC)

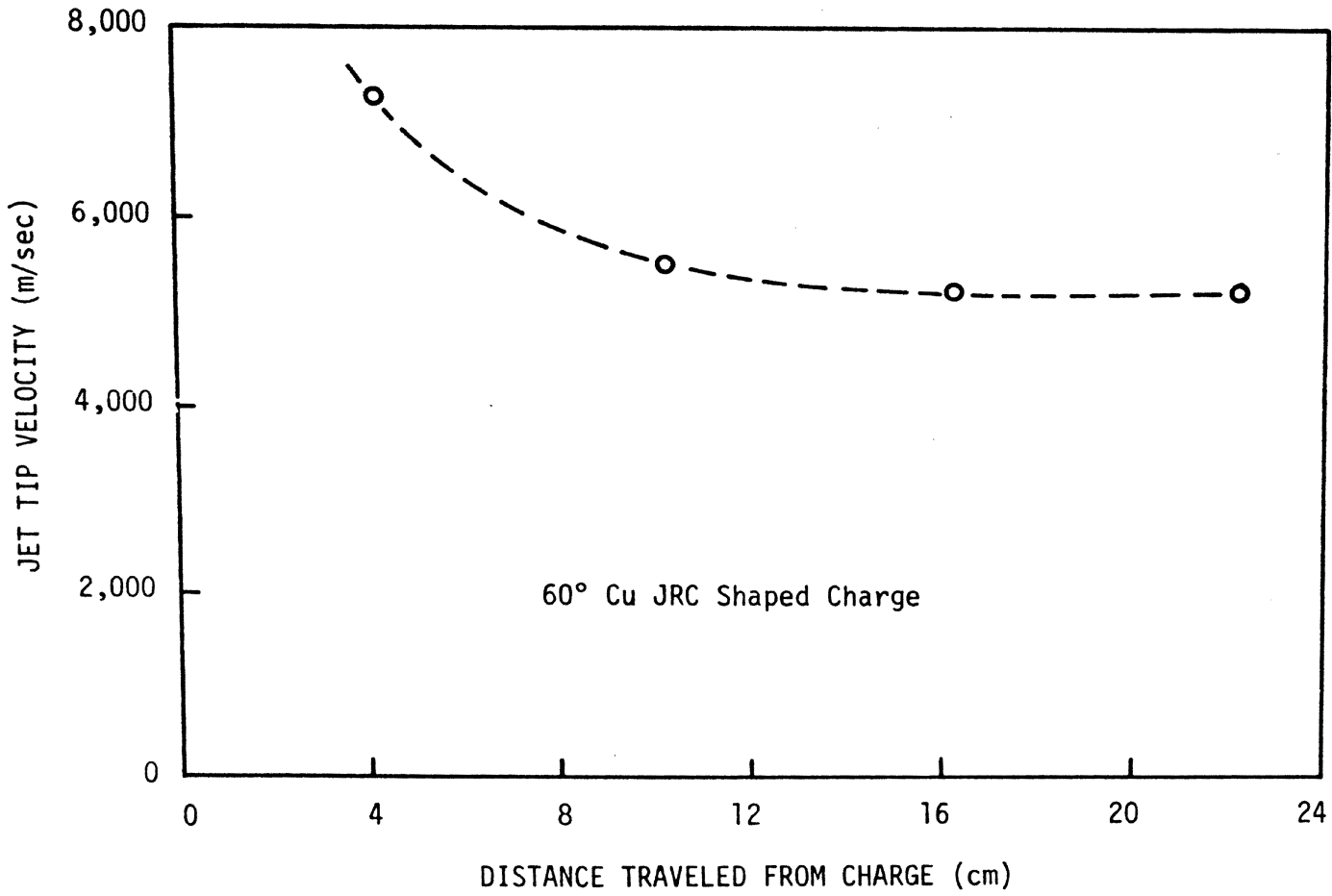


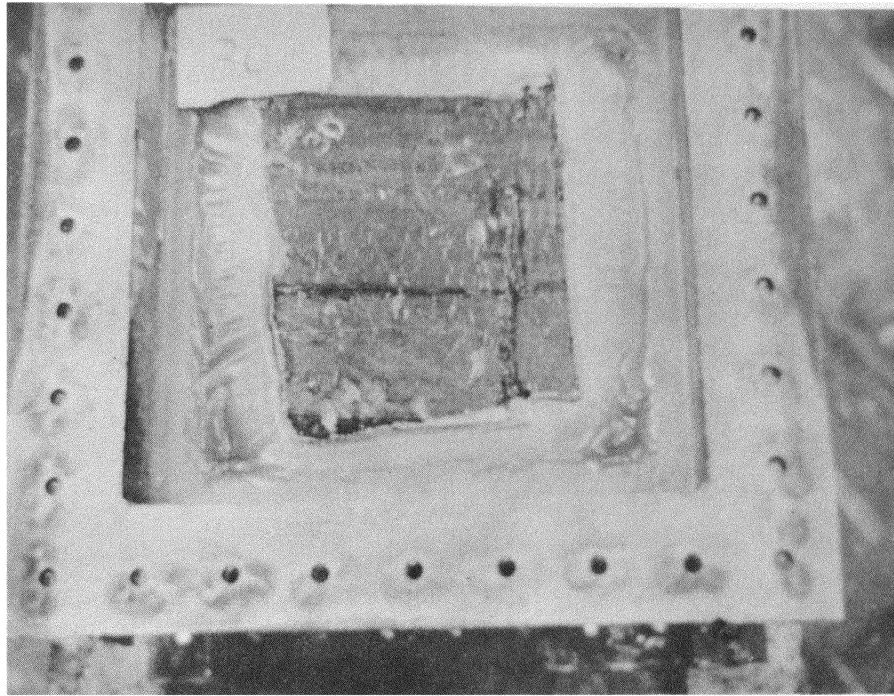
Figure 27. Jet Tip Velocity in Air (60° Copper JRC)

V. DISCUSSION OF RESULTS

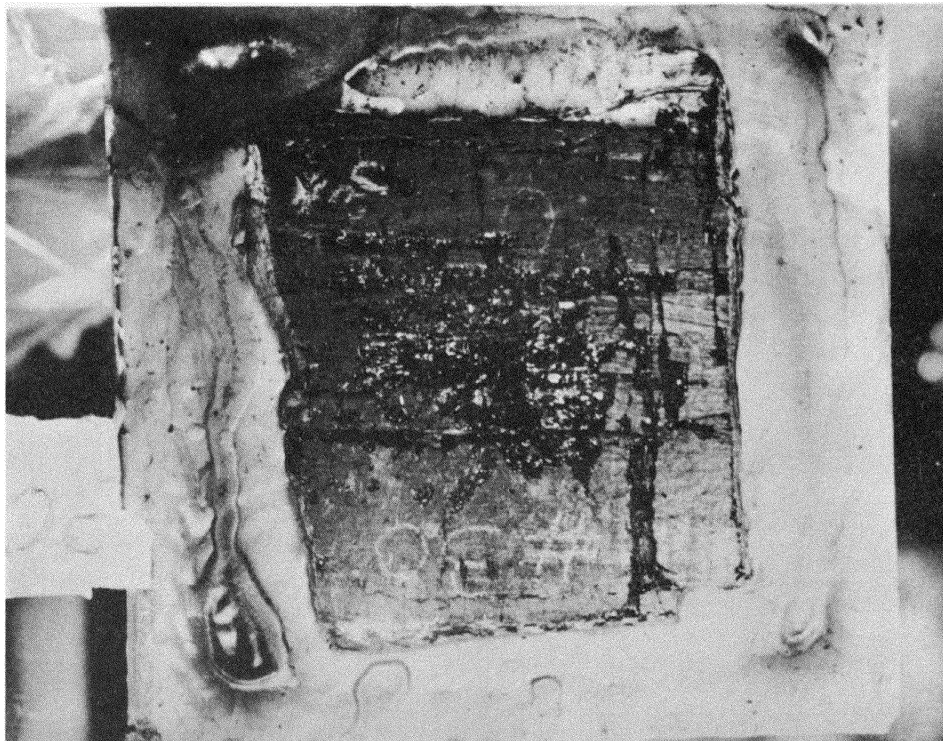
A. Permeability of Coal

Data obtained from the small samples tested indicated that gas flow parallel to the bedding planes is preferred to that across the bedding planes. Microscopic examination of small coal samples revealed a system of microfractures oriented parallel to the bedding. It must be noted, however, that laboratory testing neglects the effects of overburden pressure and therefore the extent to which these fractures are open and their effective role in gas transport in situ cannot be determined. Although microfractures existed in all large coal samples tested gas flow along the cleavage planes was 10^4 times as great as the flow through the microfracture system. Results from the use of deeper penetrating shaped charges, such as the 60° copper JRC, indicated that joints can be opened (Figs. 28 and 29) and that the rate of gas flow increases along these paths (Figs. 2 and 3). Deeper penetrating charges caused fractures to extend into the undisturbed coal. Clay veins and partings which completely seal a portion of the coal seam and render degassification methods useless can be penetrated with shaped charges without the added expense of additional drilling.

The maximum fracture formation deep within the coal blocks resulted from charges with liner apex angles of approximately 60°. The preshot permeability of coal blocks varied from 384 millidarcys to 19.25 darcys and samples taken from the same location in the coal seam varied from 1.7 darcys to 9.23 darcys. These values were randomly distributed because of the heterogeneous nature of the coal and were

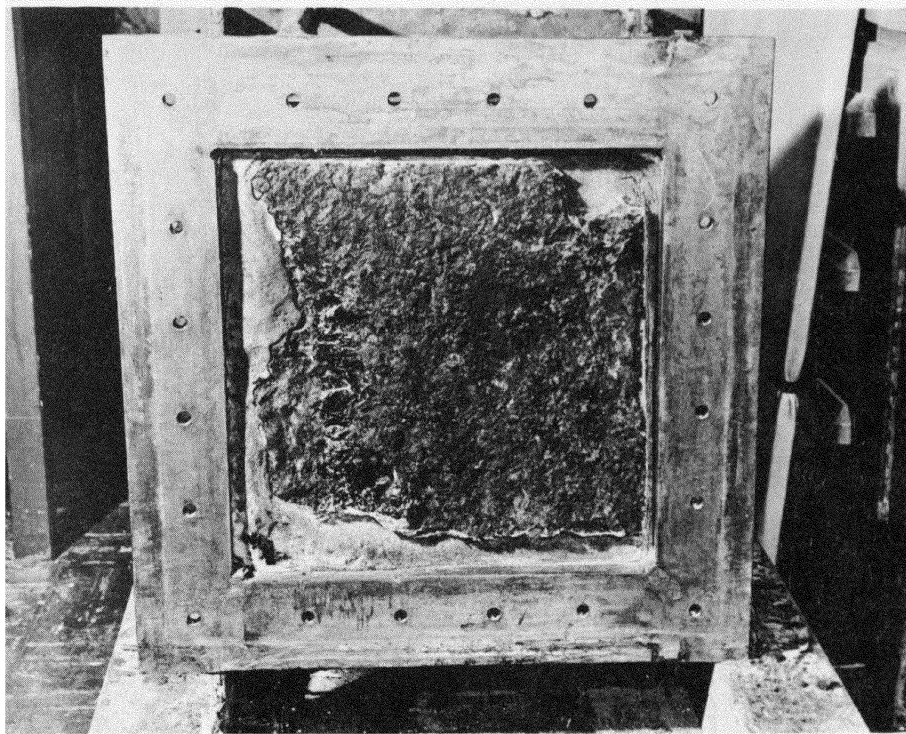


Preshot



Postshot

Figure 28. Fracture Formation Parallel to the Bedding
Due to Jet Penetration



Preshot



Postshot

Figure 29. Fracture Formation Perpendicular to the Bedding Due to Jet Penetration

dependent on the fracture system of the sample. The average postshot permeability values increased for most samples between 50 and 75 percent and the maximum increase was greater than 1,000 percent. The highest percentage increase resulted from charges using 60° and 100° copper liners.

The greatest average increase in permeability was observed for coal samples in which the jet penetration was perpendicular to the bedding planes. This would be expected because the fractures formed would normally be greater in length since they would not encounter as many discontinuities as those fired parallel to the bedding. A decrease in the post shot value was observed in four specimens which had jet penetration parallel to the bedding and no postshot decrease was observed in samples shot across the bedding planes.

The differences in permeability observed when the direction of the gas flow was reversed resulted from the fractures and jointing pattern in the coal. The gas flow in one direction tended to open fractures and joints while reversing the flow tended to close them and decrease the rate of flow through the fractures.

Data from 60°, copper, JRC charges (Figs. 2 and 3) indicate that the coal permeability increased as L_1/L decreased. This is significant because it shows that these charges cause more fractures to form at the base of the jet penetration hole rather than radially around it. This phenomenon was observed in samples shot both parallel and perpendicular to the bedding planes indicating that deep penetrating charges cause the least surface damage and result in the greatest increase in permeability.

B. Effects of Liner Material on Jet Penetration

Of the materials tested, copper or brass liners performed better than those of aluminum or titanium. Liners of titanium, copper and aluminum were tested in Plexiglas under identical conditions. The 100° copper JRC penetrated deeper than the aluminum or titanium liners. The jets from liners of aluminum and titanium made larger diameter holes than those which resulted from copper liners and caused considerable surface damage to the sample while the copper liners created fractures at depth in the target. At decreased standoffs of 0.25 CD aluminum liners failed to form a jet while copper liners formed jets with lower penetration capabilities.

Aluminum and titanium liners did not form jets in charges loaded with low velocity explosives while copper liners formed a jet for most explosives used. The weight loss of the slug was observed to increase as the velocity of the explosive increased. Of all liners tested the copper liners with 60° apex angles penetrated best and caused the greatest amount of fracturing in the target materials.

C. Effects of Detonation Velocity on Jet Penetration

Tests conducted in both dolomite and coal indicated that the jet penetration depth was a function of the detonation velocity (Figs. 24, 25 and 26).

Early shaped charge studies using ideal explosives indicated that the depth of penetration or the hole volume of shaped charge jets fired into steel targets varied directly as the detonation pressure. The detonation pressure was calculated using (30):

$$P_2 = \rho_1 DW + P_1 \quad (V-1)$$

where

P_1 = atmospheric pressure

P_2 = detonation pressure

ρ_1 = density of the unreacted explosive

D = detonation velocity

W = particle velocity

Detonation velocity (D) and particle velocity (W) are related through density by

$$W = (1 - \rho_1/\rho_2)D \quad (V-2)$$

For many practical purposes it is sufficiently accurate to assume

$$\rho_1/\rho_2 \doteq 3/4 \quad (V-3)$$

Substituting eq. (V-3) into eq. V-2

$$W \doteq D/4 \quad (V-4)$$

whereby

$$P_2 \doteq \rho_1 \frac{D^2}{4} + P_1 \quad (V-5)$$

P_1 can be assumed to be insignificant when compared to the detonation pressure. The detonation pressure in atmospheres for a detonation velocity in meters per second is

$$P_2 \doteq 0.00987 \rho_1 \frac{D^2}{4} \quad (V-6)$$

Cook (30) observed that jet penetrations for non-ideal explosives deviated from those of ideal explosives but for all except very low pressures, below 80,000 atmospheres, the penetration was directly proportional to the detonation pressure. Jet penetration depth for any explosive, holding all other parameters constant would be a

function of P_2 or D^2 . Therefore

$$P_d = f(\rho_1, D) \quad (V-7)$$

The explosives used for tests in dolomite had densities of 1.33 and 1.5 gm/cc. If the density was assumed to be constant then penetrations depths were proportional to D^2 or

$$P_d \propto K D^2 \quad (V-8)$$

where K is dependent on the properties of the rock and the liner.

Liners can collapse by either turning inside out or by collapsing toward the axis of a cone and liner geometry is considered the governing factor which determines the type of collapse which will occur. It has been observed, with low velocity explosives, that the collapse process is not strictly a function of liner geometry. Identical charges with liners of titanium and copper with 100° apex angles collapsed in different manners due to materials properties of the liner (Fig. 23).

D. Effects of Material Properties on Jet Penetration

In the derivation of the first order penetration law (Eq. III-1) the assumption was made that both the jet and target material behave as incompressible fluids and that jet penetration was strictly a function of the target density. This does not explain the difference in jet penetration in coal and Plexiglas which have almost identical densities, nor can it explain similar penetrations for lead and Plexiglas whose densities are quite different (Fig. 30). The jet tip velocity in air was measured at 5000 meters/second, yet for identical jet penetrations in coal and Plexiglas the penetration

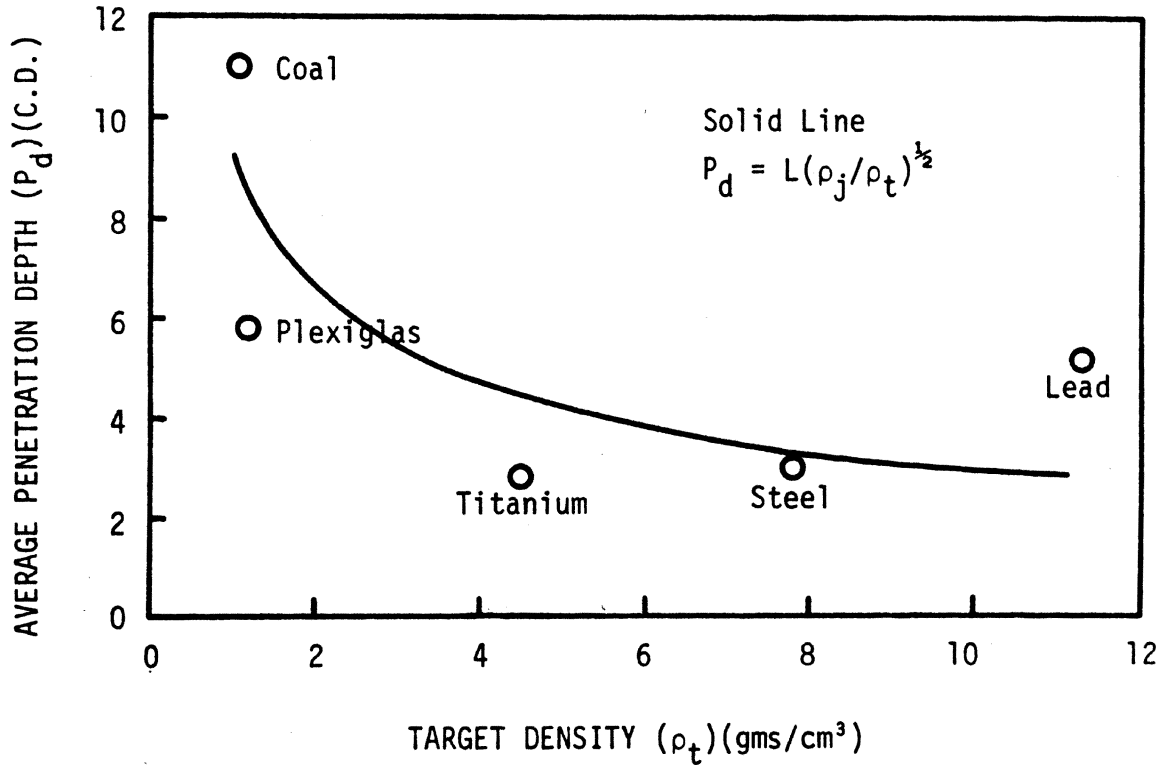


Figure 30. Average Penetration Vs Target Density for 60° Copper JRC

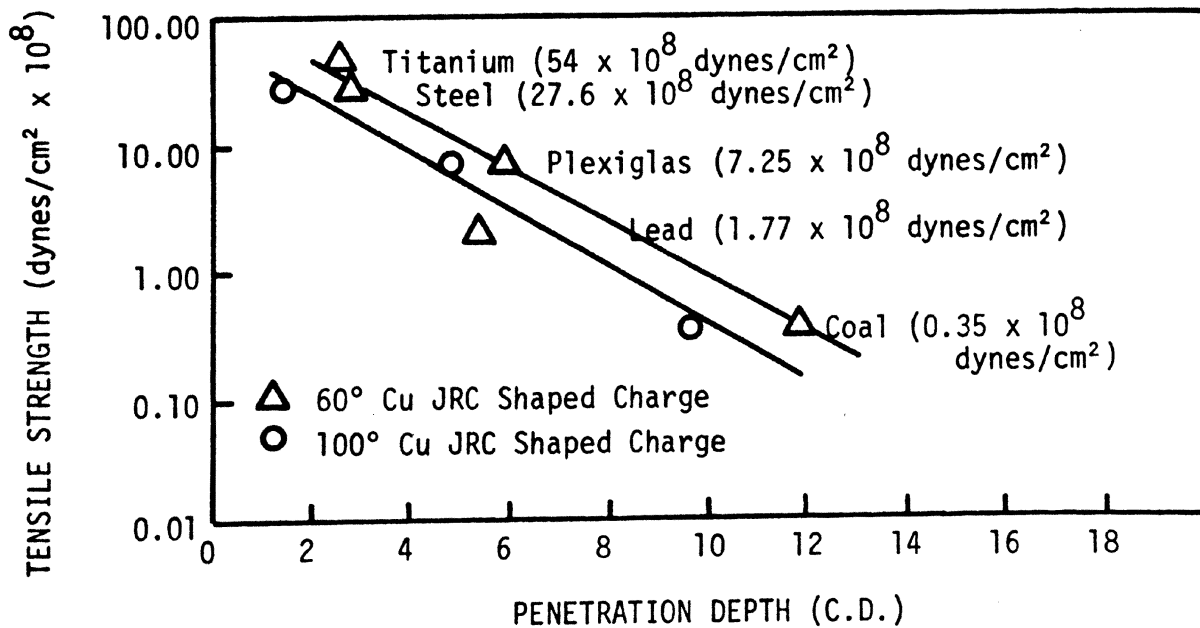


Figure 31. Tensile Strength Vs Jet Penetration

velocity was much lower in Plexiglas than that in coal (Figs. 5 and 22). This indicates that material properties other than density control the rate of jet penetration for non ideal materials. Any correction to the first order law is in the form of an empirical constant because the basis on which it was derived allows no correction for material properties.

Material properties which could be related to jet penetration depth are yield strength, Young's Modulus, wave propagation velocity, Poisson's ratio, hardness, and density.

Data obtained from the five target materials used in this study (Fig. 31) indicate that the static tensile strength of the target material is related to the jet penetration depth (Fig. 31).

$$P_d \propto \frac{1}{\ln \sigma_t} \quad (V-9)$$

where

P_d = penetration depth

σ_t = static tensile strength

Pack (32) used yield strength to correct the first order penetration law as related to metallic targets. Yield strength therefore seems to be related to penetration depth for all target materials.

The Shore hardness numbers (Appendix C) of the target materials were compared to the jet penetration distances. The data were random and no relationship between Shore hardness and jet penetration depth was observed.

Values for Young's Modulus were obtained from the literature for four of the five target materials (Fig. 32). Young's Modulus

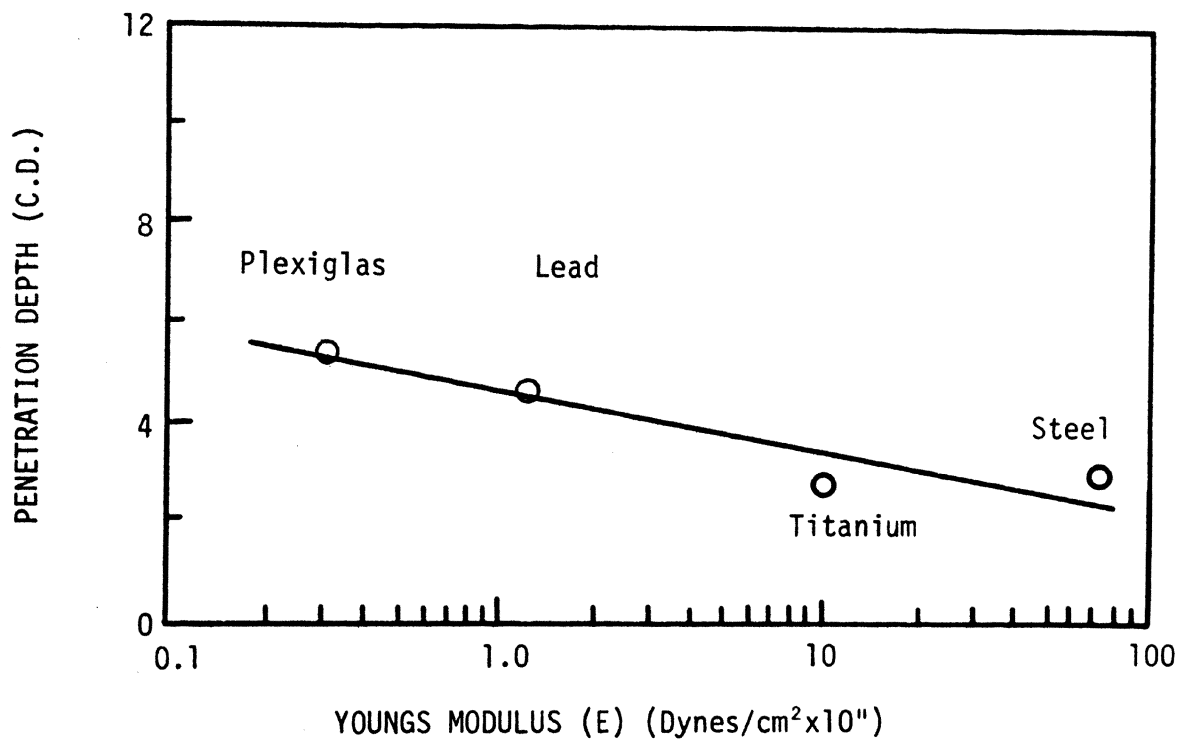


Figure 32. Penetration Depth Vs Young's Modulus

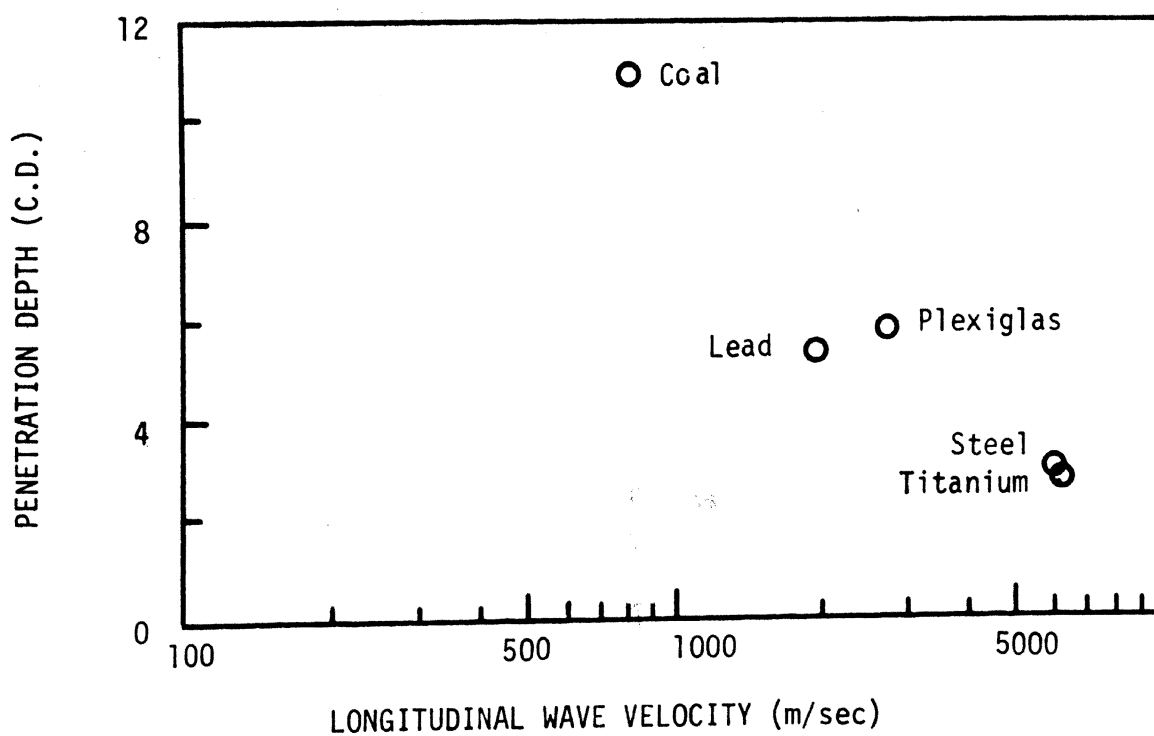


Figure 33. Penetration Depth Vs Longitudinal Wave Velocity

for coal could not be determined because of the heterogeneity of the material. Results from the four target materials, excluding coal, indicate that jet penetration depth increases as Young's Modulus decreases (Fig. 32).

$$P_d \propto \frac{1}{\ln E} \quad (V-10)$$

Jet penetration in the target material is accompanied by a rapidly deteriorating shock wave which moves ahead of the jet tip. Since material properties other than density are related to jet penetration the impact cannot be purely hydrodynamic and plastic and elastic impact must be related to the penetration process. An important parameter which governs the amount of fracturing which will occur under conditions of elasto-plastic impact is the wave propagation velocity of the material. The natural log of the wave propagation velocity through the target material is inversely related to the depth of penetration for target materials tested (Fig. 33).

$$P_d \propto \frac{1}{\ln v_p} \quad (V-11)$$

The results from the five target materials tested in this study indicate that jet penetration depth is directly related to material properties and that it is an inverse natural log function of Young's Modulus, wave propagation velocity and target yield strength.

E. Shaped Charge Effects on Homogeneous and Bedded Targets

The effects of shaped charge jets on coal and other materials which fracture in a brittle fashion must be evaluated by considering factors which relate to the properties of the target. The increase

in permeability of coal which has been fractured by shaped charge jets is not solely dependent on the penetration of the jet but rather on the fractures which are formed at a distance from the jet.

Present accepted theories on jet penetration describe failure as plastic flow of the target material. The basis for the assumption is that metal plates penetrated by jets show negligible weight loss. In homogeneous materials the jet has always been observed to penetrate along the jet axis with no deviation from a straight line. The jet penetration hole in coal, however, was observed to deviate considerably from a straight line (Figs. 19 and 21). This deviation would be impossible if materials properties were insignificant and if the impact was totally hydrodynamic.

1. Stress Waves and Impulse Loads

Impact loading on target materials is a function of a number of different mechanisms, which determine the nature of penetration and the stress wave patterns generated in both the projectile and the target.

a. Elastic Impact

When impact velocities are sufficiently low, the stress in the target material does not exceed the proportional limit, and the nature and duration of the impact will depend on the elastic constants and elastic wave velocities of the material. Three types of elastic waves are generated in the target: a dilatational wave, a distortional wave and a Rayleigh (surface) wave. An ideal medium stores the kinetic energy received in an impact as elastic strain energy. The whole

process is reversible and nearly all the stored elastic strain energy is converted back into kinetic energy as the projectile rebounds at a velocity near its approach velocity.

b. Plastic Impact

The yield point of the material will be reached at the critical velocity and plastic deformation will occur. As the velocity progressively increases above the critical velocity a greater portion of the kinetic energy of the projectile is expended in plastic work in the target and the elastic deformations decrease in importance.

Brittle target materials are an exception and react differently to increased impact velocity (34). Materials which deform plastically do so because shear stresses exceed the yield point while actual fractures are produced in brittle materials when tensile stresses exceed the ultimate tensile strength.

c. Hydrodynamic Impact

When stresses in a material greatly exceed its yield strength either the target or the projectile or both can be regarded as fluids. In this case elastic and strength properties become insignificant and target and projectile densities influence the nature of the impact. This approach has been used to describe the penetration of shaped charge jets into "hard" materials. Jet penetration in viscoelastic materials such as hard glasslike plastics, however, is dependent on material properties rather than density (34) because dynamic strengths of these materials far exceeds their static strength and rapid slip deformations cannot occur along crystalline glide planes

as they do in metals.

2. Fracture Mechanics

When a stress pulse of sufficient magnitude and short duration travels through a brittle solid, fracture phenomena are different in several respects from those produced under static loading conditions. When a static load is applied to a specimen the tensile strength is a measure of the worst flaw, since fractures will initiate at this location. Under conditions of dynamic loading, however, fractures can be initiated in a number of locations simultaneously. In the case of loading by stress waves, fractures can form at many nuclei but since fracture propagation velocity is low in comparison to the velocity of the stress wave, the fracturing soon ceases because the stress wave has passed and the load has been relieved from the fracture (34).

The observed tensile strength of many brittle materials is found to depend on the flaws in the surface of the specimen. Under static loading conditions it is impossible to stress the interior of the specimen without also stressing its surface. In dynamic loading, however, samples can be internally stressed while the surfaces remain stress free. Tensile strengths of many materials are found to vary inversely with the loading time. Therefore, material under dynamic loading conditions for 1 - 2 μ sec can have a higher tensile strength value than a sample loaded statically for a longer period of time.

When a compressive stress is incident on a free face boundary in an elastic medium, it produces a reflected tensile pulse at that boundary. The distance from the free boundary to the point where

maximum tension will first develop will depend on the shape of the initial stress pulse. This distance has been found to be between zero and one-half the total pulse length from the free boundary (35). For an initially symmetrical pulse it is found to occur at a distance one-quarter the pulse length from the free boundary.

A 100° copper JRC charge was fired at a 45° angle to the discontinuities in a laminated Plexiglas model (Fig. 13). A reflected tensile slab was observed to form directly beneath the point of initial impact. The distance from the free boundary was found to be 0.279 cm which corresponds to a pulse length of at least 2 μ sec. If the jet impact is considered to form a symmetric pulse, then it would have a duration of 4 μ sec.

The static tensile strength of Plexiglas is about 20 times that of coal. The effect of the compressive stress wave in coal is to produce greater breakage at the bedding planes. The discontinuities (bedding) in coal, however, are considered as a density discontinuity but not truly a free boundary, therefore, stress waves are not totally reflected and some are refracted into the next layer. The refracted wave reaches other bedding planes and is subsequently reflected and refracted with tensile fracture possible at the boundary. A complex stress wave system results from these reflected and refracted waves. Breakage occurs at each discontinuity until the amplitude of the wave becomes insufficient to cause further fracturing and elastic behavior results. Distortional waves are responsible for less fracturing than that resulting from dilatational waves since the amplitude is normal to its direction of motion.

Vertical discontinuities in coal (joints) have the same effect

as bedding on the stress waves. Joints which are physically separated function as a free boundary and stress waves are almost totally reflected.

Fracturing in coal near the jet penetration has been observed to be intense and is usually bounded vertically by the joints with major fracturing confined between sets of jointing planes. The coal breaks into large and small pieces, usually parallelepipeds, which follow the natural cleavage planes. Some large fractures are observed to cross joints and travel long distances in the coal. Fractures originating at the base of the jet penetration also travel across the bedding planes and continue deeper into the sample. Calcite deposits in vertical joints have been shattered at a distance from the charge due to the reflected stress waves.

Fracturing laterally around the jet penetration in Plexiglas is a twofold system. The material is observed to form a plastic zone near the collar of the hole, and decreases in diameter along the length of penetration (Fig. 16). Fractures originated at the outer boundary of this zone approximately 12 μ sec after impact and proceeded only a short distance. Maximum fracture velocity was observed to be 1040 meters/second which is approximately the shear wave velocity in the material. Fracturing ceased because the compressive wave velocity was much greater than the fracture propagation velocity and stress was removed from the fracture tip as the compressive wave passed. Large radial fractures were formed at a later time due to trapped strain energy resulting from the high gas pressures associated with the explosive charge. Jet penetration at the interface between two large Plexiglas blocks produced no large

radial fractures because pressure could be relieved at the interface along the jet axis (Fig. 16).

No plastic zone was observed for jet penetrations in coal but a crushed zone did exist immediately around the jet penetration hole. Radial fracturing along the jet penetration path in coal should be less in proportion to that in Plexiglas since the shear wave velocity is lower and the compressive wave more quickly outdistances the fracture propagation. Breakage in coal was more pronounced than in Plexiglas due to the very low tensile strength of the material. Kolsky (34) states that fracturing should be greater near the base of the jet penetration because the impulse is traveling near the fracture velocity of the material, and fracture tips are moving in a stressed area causing longer fractures to form.

Fracture propagation velocity was measured in Plexiglas models using MDF and found to be 1040 meters/second near the charge and decreased to about 700 meters/second at a distance of a few centimeters. Kolsky has reported similar velocities (34). The maximum fracture velocity in Plexiglas approaches the shear wave velocity of 1100 meters/second.

The fracture profile caused by MDF and shaped charges was U shaped in a homogeneous medium. Fracture profiles in laminated models were different than those in homogeneous models since tensile reflections from discontinuities were an important breakage mechanism (Figs. 9 and 10). When MDF or shaped charge jets were fired parallel to discontinuities in laminated models no fractures were observed to cross the discontinuities and fracturing was confined to a small area (Figs. 11 and 12).

Shaped charges cause less lateral breakage than conventional charges because the stress pulse is short in duration and fracturing is basically due to the shock wave originating from the jet penetration. Conventional explosives produce a shock wave in the material and also stress the material for a longer duration due to the high gas pressure. Fracturing at the base of the shaped charge hole is greater in extent than those produced by conventional explosives.

3. Mechanics of Penetration in Coal

Jet penetration profiles are characterized by a crushed and compacted zone immediately around the hole. A well fractured zone exists beyond the crushed zone, followed by a zone of radial fractures (Figs. 19, 28 and 29). Shaped charge jets were fired into coal samples, with a steel blast shield used to protect the sample from the effects of the charge. Larger quantities of coal dust were observed on the surface of the coal near the point of jet impact. The surface crater in the coal was filled with small coal particles and the dust resulted from the jet penetration. The finest dust grains which could be observed under 320 power microscopic examination indicated that brittle fracture was the mechanism of breakage. Concoidal fractures along with separation along cleavage planes indicate that the material failed in tension or shear and was ejected from the hole during the penetration process.

The jet penetration path in relatively homogeneous materials is linear while the penetration path of 60° JRC charges in coal has been observed to be nonlinear. The present theory of shaped charge penetration states that the target material at the jet tip flows

plastically away from the tip allowing the jet to penetrate into the target. This flow is assumed to occur because the calculated pressure at the jet tip is many times the yield strength of the material and hydrodynamic impact is assumed to occur. Nonlinearity of the jet penetration path in a heterogeneous brittle target material suggests that penetration phenomena are not totally hydrodynamic in nature and DiPersio (36) has observed that jet penetration depth is a function of the hardness of the target and not its density.

VI. CONCLUSIONS

Gas flow through the microfracture system in coal is dependent on bedding orientation and is greater parallel to the bedding planes. The fracture permeability of the large joints is greater than that of the microfractures, consequently, they are responsible for the majority of gas flow through the coal seam. Shaped charges fired perpendicular to the bedding planes increased the effective permeability to a greater extent than those fired parallel to the bedding. Jet penetration depths, however, decreased as the jet crossed bedding planes. A jet penetration of 11 CD resulted from the use of 60° copper liners while other liners tested produced penetrations of approximately 7 to 8 CD. The surface damage in the model which resulted from the use of this liner was also less than that of all other liners tested.

Discontinuities parallel to the jet penetration axis in both coal and Plexiglas confined intense fracturing to a region between them, while large fractures did cross discontinuities in coal samples. Tensile fractures which resulted from stress pulses reflected at discontinuities were observed in laminated Plexiglas models when jet penetration was perpendicular to the discontinuity.

Small shaped charges (1.27 cm diam) loaded with low velocity permissible explosives did not function as well as 4.76 cm diameter charges since the grain size of the explosive could not be scaled, therefore, the grain size distribution effected liner collapse in small charges. Dolomite was used as a target material for penetration tests utilizing charges of 4.76 cm diameter since coal blocks of the necessary large size were not available. The depth of jet

penetration in both coal and dolomite was proportional to the detonation velocity of the explosive used. The depth of the surface crater formed by shaped charge impact was inversely proportional to the jet penetration depth. Negligible fracture formation and penetration resulted from shaped charges with unlined cavities. The deepest penetration obtained was 38 cm for a jet from an 80° brass cone and composition C4.

Standoff distance was critical for charges with aluminum liners. At a standoff distance of 0.25 CD copper lined charges formed jets with decreased penetration capabilities while aluminum lined charges did not form a cohesive jet. Physical properties of liner materials influenced liner collapse mechanisms in charges loaded with low velocity explosives. Copper liners with 100° apex angles collapsed uniformly about their axis while similar liners of titanium turned inside out.

A nonlinear jet penetration hole was observed in coal and microscopic examination of coal particles adjacent to the jet penetration and dust resulting from the penetration indicate that jet penetration depth is highly dependent on the properties of the target. Jet penetration depth was observed to be inversely proportional to the static tensile strength, Young's Modulus, and the longitudinal wave velocity of the target.

REFERENCES

1. Cervik, J., "An Investigation of the Behavior and Control of Methane Gas," Mining Congress Journal Reprint, July, (1967).
2. Cervik, J., "The Methane Problem," Technical paper presented at Methane Control Research Meeting, Pittsburgh, Pennsylvania, (1969).
3. Scheidegger, A. E., The Physics of Flow Through Porous Media, Rev. ed., University of Toronto Press, (1960).
4. Sevenster, P. G., "Diffusion of Gases Through Coal," Fuel, V. 38, (1959).
5. Cervik, J., "Behavior of Coal-Gas Reservoirs," Technical Progress Report - 10, Bureau of Mines, (1969).
6. Merritts, W. M., "Recent Research in Degasifying a Coalbed Before and During Mining," International Symposium on Mining Research, Rolla, Missouri, (1961).
7. Ammsov, I. I., and Eremim, I. V., Fracturing in Coal, Israel Program for Scientific Translations Ltd., Jerusalem, Distributed by International Scholarly Book Service, Inc., P. O. Box 4347, Portland, Oregon, (1963).
8. Eichelberger, R. J., "Re-Examination of the Theories of Jet Formation and Target Penetration by Lined Cavity Charges," Ph.D. dissertation, Carnegie Institute of Technology, Pittsburgh, (1954).
9. Clark, G. B., "Studies of the Design of Shaped Charges and Their Effect in Breaking Concrete Blocks," American Institute of Mining Engineers, Technical Paper 2157, (1947).
10. Austin, F. C., "Lined-Cavity Charges and Their Use in Rock and Earth Materials," New Mexico Institute of Technology, Bulletin 69, (1959).
11. Hutt1, J. B., "The Shaped Charge for Cheaper Mine Blasting," Engineering and Mining Journal, Vol. 147, (1946).
12. Kalia, H. N., "Penetration in Granite by Shaped Charge Liners of Various Metals," Unpublished Ph.D. dissertation, University of Missouri-Rolla, Rolla, Missouri, (1970).
Published as: Clark, G. B., Rollins, R. R., Brown, V. W., Kalia, H. N., "Rock Penetration by Jets From Lined Cavity Explosive Charges," Proceedings of the Twelfth Symposium on Rock Mechanics, Rolla, Missouri, (1970), Port City Press, Baltimore (1971).

13. Recommended Practices for Determining Permeability of Porous Media, API RP27, Dallas, Texas, (1956).
14. Amyz, J. W., Bass, D. M., Jr., and Whiting, R. L., Petroleum Reservoir Engineering, McGraw-Hill Co., New York, (1960).
15. Klinkenberg, L. J., "The Permeability of Porous Media to Liquids and Gasses," American Petroleum Institute, Central Committee on Drilling & Production Practices, (1941).
16. Fulton, P. F., "The Effect of Gas Slippage on Relative Permeability Measurements," Producers Monthly, V. 15, N. 12, (1951).
17. Steward, C. R., Craig, F. F., Jr., and Morse, R. A., "Determination of Limestone Performance Characteristics by Model Flow Tests," Transactions of A.I.M.E., Vol. 198, (1953).
18. Steward, C. R., and Owens, W. W., "A Laboratory Study of Laminar and Turbulent Flow in Heterogeneous Porosity Limestone," Petroleum Transactions of A.I.M.E., Vol. 213, (1958).
19. Mangunwidjojo, A. S., "Effects of Size and Shape of Specimens and Gas Slippage Phenomena in the Measurement of Coal Permeability to Gas Flow," Unpublished M.S. thesis, Virginia Polytechnic Institute, Blacksburg, (1967).
20. Lin, J. P., "Fracture Effect on Coal Permeability," Unpublished M.S. thesis, Virginia Polytechnic Institute, Blacksburg, (1966).
21. Wang, Y. J., "Effects of Specimen Size on Permeability Measurements of Gas Flow in Coal," Unpublished M.S. thesis, Virginia Polytechnic Institute, Blacksburg, (1962).
22. Huang, M. S., "A Study of the Permeability of Coal to the Flow of Gas," Unpublished M.S. thesis, Virginia Polytechnic Institute, Blacksburg, (1961).
23. Koo, S. M., "A Study of the Factors that Affect the Permeability of Coal," Unpublished M.S. thesis, Virginia Polytechnic Institute, Blacksburg, (1960).
24. Lowry, H. H., Chemistry of Coal Utilization, John Wiley & Sons, Suppl. Vol., New York, (1963).
25. Karn, F. S., Friedel, R. A., and Sharkey, A. G., Jr., "Diffusion Studies of Light Hydrocarbon Gases Through Coal," Bureau of Mines RI 7441, (1970).
26. Nandi, S. P. and Walker, P. L., Jr., "Diffusion of Argon from Coals of Different Rank," Coal Science, ACS, Washington, (1966).
27. Perkins, J. H., and Cervik, J., "Sorption Investigations of Methane on Coal," Bureau of Mines, T. P. Report-14, (1969).

28. Elder, C. H., "Use of Vertical Boreholes for Assisting Ventilation of Longwall Gob Areas," Bureau of Mines, T. P. Report 13, (1969).
29. Kickovic, S., Findlay, C., and Merritts, W. M., "Methane Emission Rate Studies in a Northern West Virginia Mine," Bureau of Mines, T. P. Report 28, (1970).
30. Cook, M. A., The Science of High Explosives, Reinhold Publishing Corporation, New York, (1958).
31. DiPersio, R., Simon, J., and Merendino, A. B., "Penetration of Shaped Charge Jets into Metallic Targets," BRL 1296, Aberdeen Proving Grounds, Maryland, (1965).
32. Pack, D. C., and Evans, W. M., "Penetration by High Velocity ('Munroe') Jets I," Proc. of the Physical Society, London, Vol. B64, (1951).
33. Pugh, E. M., and Eichelberger, R. J., "Crater Formation in Metals by High Velocity Fragments," First Hypervelocity Impact Symposium, Santa Monica, (1955).
34. Hopkins, H. G., and Kolsky, H., "Mechanics of Hypervelocity Impact of Solids," Symposium on Hypervelocity Impact, April, (1960).
35. Kolsky, H., and Rader, D., "Stress Waves and Fracture," Fracture, Vol. 1, Academic Press, New York, (1968).
36. DiPersio, R., and Simon, J., "Resistance of Solid Homogeneous Targets to Shaped Charge Jet Penetration," BRL Rept. 1417, October, (1968).
37. Klamer, O. A., "Shaped Charge Scaling," AD 600 273, Picatinny Arsenal, Dover, New Jersey, (1964).
38. Zernow, L. and Simon, Jr., "High Strain Plasticity of Liner Metals and Jet Behavior," Transactions of the Symposium on Shaped Charges, BRL (AD 58 899), Aberdeen Proving Grounds, Maryland, (1953).
39. Bell, W. T., "The New Titanium-Lined Shaped Charge Perforation," Oil & Gas Journal, November, (1962).
40. Brimmer, R. A., "Manual for Shaped Charge Design," Navord Report 1248 (ATI 84 949), China Lake, California, (1950).
41. DiPersio, R., "Characteristics of Jets from Small Caliber Shaped Charges with Aluminum and Copper Liners," BRL Memo. Rept. 1866, September, (1967).

VITA

Calvin Joseph Konya was born on June 23, 1943 in Cleveland, Ohio. He received his primary and secondary education in Cleveland. As an undergraduate he received the Don B. McCloud Memorial Fund Scholarship for two years. He received his Bachelor of Science Degree in Mining Engineering in August 1966 from the University of Missouri at Rolla (UMR).

As a graduate student he held a graduate assistantship in the Department of Mining Engineering. He also received a National Defense Education Act Grant Fellowship for three years. Since September 1970 he has been associated with the Rock Mechanics and Explosives Research Center as a Senior research assistant.

The author received his Master of Science in Mining Engineering in May 1968, from UMR. He received a second Master of Science in Engineering Management in August 1970 from UMR.

APPENDIX A

EXPERIMENTAL DESIGN

The validity of data which results from a permeability study depends on the correct choice of sample size in a heterogeneous material and the method of sample preparation. Incorrect sample size or sample preparation methods which change the physical properties of the material would negate the validity of the results. For this reason special emphasis was placed on sample size and preparation in this study.

A. Selection of Coal Model Size

The dimensions of the coal test blocks were determined by the following factors:

1. Penetration depth of jet
2. Ease of encapsulation
3. Geologic features in coalbed
4. Ease of obtaining undisturbed coal specimens

1. Penetration Depth of Jet

Preliminary penetration tests were conducted on two coal blocks confined in wet sand to offer some lateral restraint.

Shaped charge liners of 1.27 cm and 1.59 cm diameter with 60° apex angles were made of yellow brass and were placed in charges utilizing composition C4 as the explosive. The 1.59 cm diameter gave the greatest penetration, which was 12.06 cm or 7.6 cone diameters.

2. Ease of Encapsulation

The difficulties of encapsulation in a steel confining chamber increased with the volume of the sample. The coal blocks were coated with an epoxy resin and encapsulated in wax inside a steel chamber with removable end plates. Wax (paraffin) was found to be impermeable and to bond well to both the sealed coal and steel. Disassembly of the model was accomplished by heating the chamber until the model slid out under its own weight.

3. Geologic Features in Coalbed

As many geologic features as possible, including joints, were included in the models in order that typical gas flow in natural fracture systems could be investigated.

One set of coal blocks was obtained from a site in north central Missouri, but the samples were unsatisfactory due to fractures caused by the mining method. The Illinois number 6 seam was then considered as a possible source of samples. The jointing pattern for this coal was on the order of 7.5 cm (Appendix D).

4. Ease of Obtaining Undisturbed Coal Specimens

A 30.5 cm coal cube was found to satisfy the size requirements without being too large to handle. Coal samples were obtained from an underground mine which used conventional mining methods. This coal was found to be unsatisfactory because calcite filled joints were shattered by the use of Airdox in the mining method.

Usable coal blocks were obtained from the Inland Steel mine near Sesser, Illinois. The mine is operated using continuous mining

machines and therefore the coal is undisturbed in the face. Samples were cut from a face in virgin coal which had been exposed for a minimum period of time, less than 24 hours. The coal was stress relieved by cutting a kerf along the top of the seam before samples were cut. Samples were sealed in plastic bags and stored at 20°C until used.

B. Preparation of Coal Model

A masonry saw with a 36 in. diameter blade was first employed to trim the models to the correct size for encapsulation. This method of cutting wet was abandoned because the water tended to wash out fine material from joints and bedding planes. It also reduced the tensile strength between some bedding planes causing the samples to fall apart.

To approximate in situ conditions as nearly as possible, a dry cutting technique was employed. A Homelite XL-12 chain saw was used to cut large blocks, but it did not have the capability to be used as a trim saw. A metal cutting Wellsaw, Model 8, with a bimetal blade was used to trim the coal models to size, cutting coal, pyrite, and shale bands with equal ease.

The cut coal samples were brushed clean and the four sides which would later be covered with wax were coated with E-2 Epoxy adhesive manufactured by the Sealoid Company. The sample was then sealed in a metal chamber (Fig. 34) with melted wax. No attempt was made to dry the sample and remove its natural moisture content. It was felt that heating a large sample above 100°C would change the coal sufficiently to induce more error in the permeability

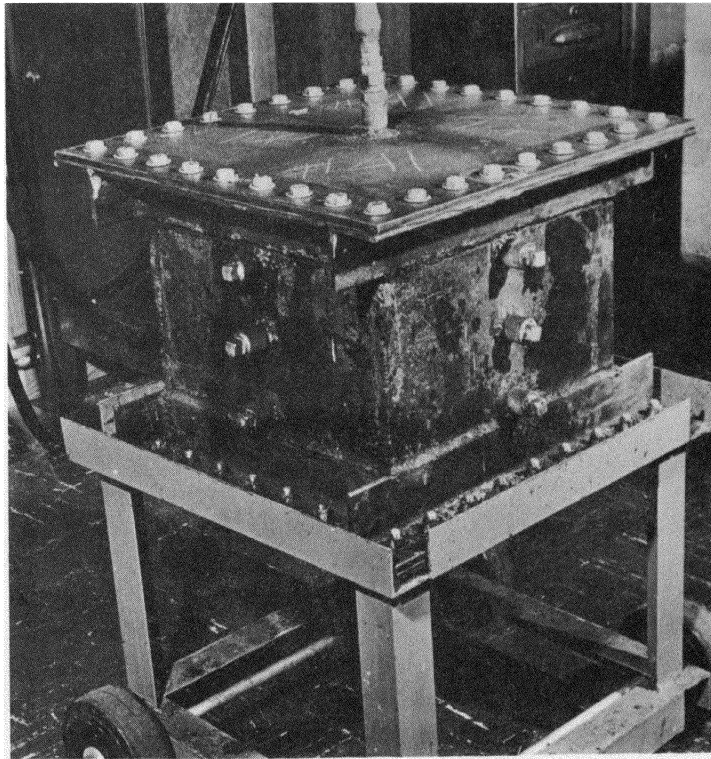


Figure 34. Sample Holder for Large Specimens

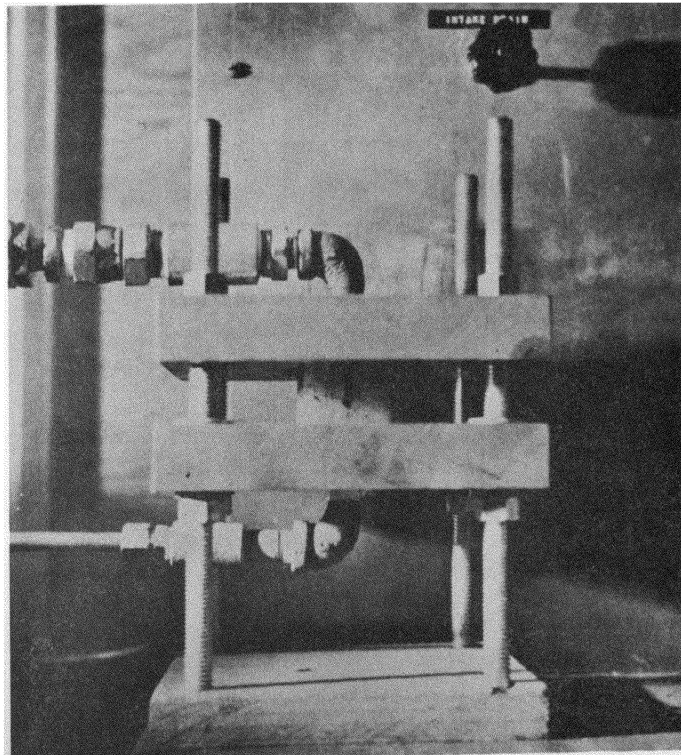


Figure 35. Sample Holder for Small Specimens

measurements than those which would result from the moisture. The two faces which were to be tested for gas flow permeability were left as received from the sawing operation. The encased model and box weighed over 400 lbs. A small sample holder for permeability measurements was also constructed to accommodate samples less than 5 cm by 5 cm (Fig. 35).

C. Permeameter

The permeameter consisted of: a source of dry compressed air; two U tube mercury manometers; two U tube water manometers; flowmeter, Lab Crest Century Series 100, flow range from 0.4 to 23,400 cc/min; a barometer and thermometer (Figs. 36 and 37).

D. Flash X-ray Equipment

Two, 600 kv, 730-2660 series, flash X-ray units (Field Emission Corporation) were employed to take radiographs as the shaped charge jet penetrated the coal. From these radiographs shaped charge induced fractures were observed and jet penetration velocities were calculated.

E. Framing Camera

A Cordin model framing camera with a maximum framing rate of 1.25×10^6 frames per second was used to record penetration phenomena of shaped charges in Plexiglas. Models simulating bedded and homogeneous deposits were photographed.

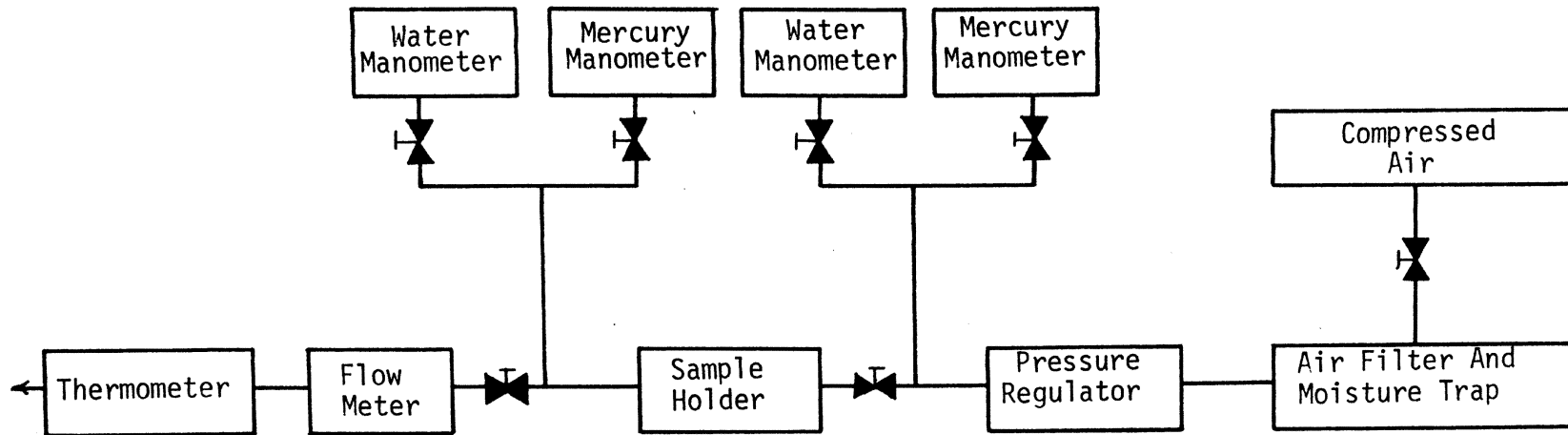


Figure 36. Diagram of Permeameter

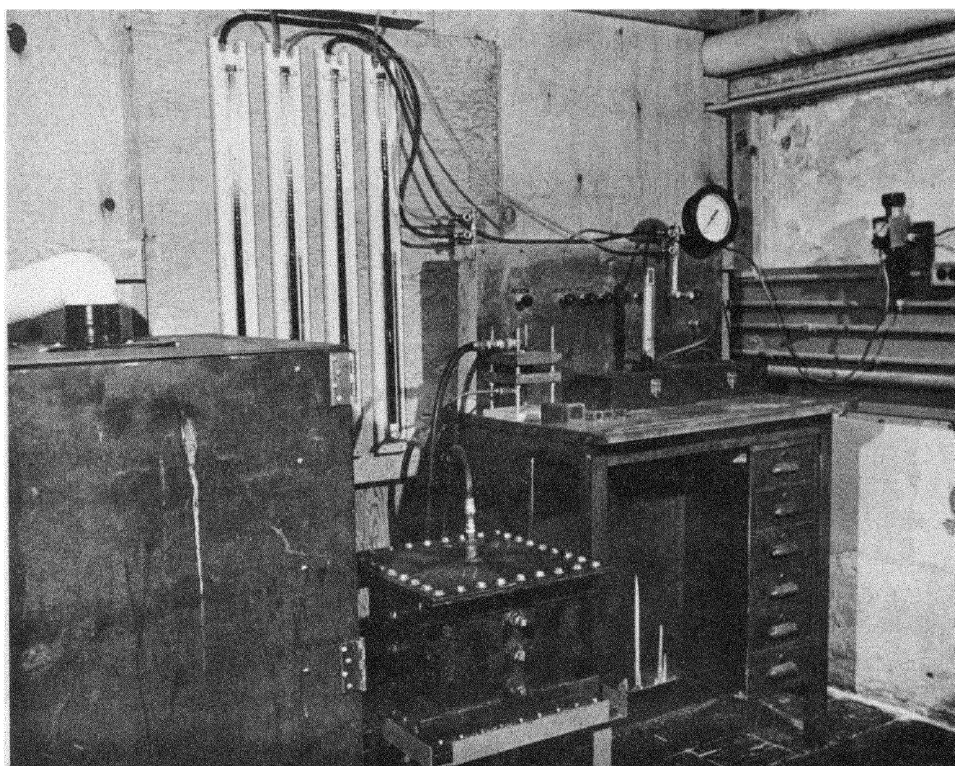


Figure 37. Permeameter Assembly

F. Shaped Charge Design

A concise summary of shaped charge design for military purposes has been given by Klammer (37). The following parameters were considered in the design of the shaped charges for this investigation:

1. Liner material
2. Liner apex angle
3. Type and velocity of explosive
4. Charge dimensions
5. Standoff

1. Liner Material

After testing several metals, Zernow (38) concluded that jets of face centered cubic metals all stretch more or less taffy-like in flight, body centered cubic metals show early fracture into large pieces and hexagonal metals fracture early into small pieces. Low melting point metals generally form a broad dispersed spray-like jet, a common behavior independent of their crystal structure. Metals such as copper, nickel, aluminum, and silver behave similarly and are all face-centered cubic in crystal structure. Iron is body-centered cubic in structure while metals such as magnesium, cobalt, and titanium are hexagonal in structure. Titanium slowly changes its crystal structure from hexagonal to cubic when raised to temperatures above 880°C.

Oil well perforation experiments (39) have shown that some jet materials react with the target medium producing exothermic reactions and increasing lateral pressures around the holes. Titanium jets

fired into limestone created fractures extending beyond the hole, which were not present for other metal jets such as zinc, lead, copper, or steel. Liner materials used for this study included brass, copper, aluminum, and titanium.

2. Liner Apex Angle

The optimum cone apex angle was shown by Brimmer (40) to be near 60°. Borehole degasification techniques involving 7.5 cm diameter boreholes would limit the height of the charge. The cone diameter could be increased only by increasing the cone angle. Liners utilizing 60°, 80° and 100° cone angles were used in this investigation.

3. Type of Explosive

Explosives with velocities in the neighborhood of 8,000 meters per second are normally used in shaped charges to maximize the detonation pressure and jet penetration depth. This study included explosives having velocities between 1,800 and 8,100 meters per second. Both high explosives and coal mine permissibles were used (Table XIV).

4. Charge Geometry

Long, cylindrical, explosive charges of three to four charge diameters produce maximum penetration, while beehive shaped charges of shorter dimensions give greater penetration per unit weight of explosive (30).

DiPersio (41) found that penetration of shaped charge jets from aluminum and copper does not scale for charges less than 5 cm in diameter. Therefore, the penetration of a 1.27 cm diameter charge

TABLE XIV
EXPLOSIVE'S PROPERTIES

<u>Explosive</u>	<u>Type</u>	<u>Density (gm/cc)</u>	<u>Velocity Unconfined (meters/sec)</u>
Composition C4	H.E.	1.50	8040
Cyclonite (RDX)	H.E.	1.65	8180
Dupont 40 Spec. Gel.	H.E.	1.60	3048
Atlas Coalite 5Y	permissible	0.83	1828
Atlas Coalite 5U	permissible	1.07	2590
Atlas Gelcoalite Z	permissible	1.33	4267

is less than one-half the penetration of a 2.54 cm diameter charge.

Model size restrictions dictated that charges with cone diameters of 1.27 cm would be necessary. Hand-loaded cylindrical charges were employed together with selected commercially available charges purchased from the Jet Research Center (JRC) (Table XV). The JRC charges were machine-loaded and the explosive was pressed to 100,000 psi. Although the length-to-diameter ratio of these charges was approximately 1.0, their penetration capabilities were similar to hand-loaded cylindrical charges having length-to-diameter ratios between two and three. A uniform loading density due to pressing at high pressures could account for this.

The JRC charges were fired into granite (Table VII) and the scaled penetration exceeded conventionally designed cylindrical charges employed by Kalia (12).

The geometry of the JRC charges would be similar to those utilized in a borehole degasification system. Penetration tests in steel using one cone diameter standoff were conducted by the Jet Research Center to determine jet penetration characteristics. Jets from liners of titanium and aluminum with 100° apex angles gave the largest diameter holes while the jet from a 60° copper liner gave the greatest penetration (Table XVI).

5. Standoff

Borehole degasification applications would impose limits on charge height. This may be a critical factor in the use of aluminum liners because the optimum standoff for aluminum is greater than for either copper or brass. Optimum standoff could only be achieved for charges with small cone diameters.

TABLE XV
JRC CHARGE DATA

<u>Charge Designation</u>	<u>Liner Material</u>	<u>Liner Angle (deg)</u>	<u>Charge Diameter (in.)</u>	<u>Liner Thickness (in.)</u>	<u>Explosive Weight (gm)</u>
C-1725-5	Cu	100	0.5	0.021	1.1
C-1725 Special	Cu	60	0.5	0.019	1.2
C-1726-5	Al	100	0.5	0.050	1.1
C-1727-5	Al	80	0.5	0.420	1.1
Special*	Ti	100	0.5	0.021	1.1
C-2525	Cu	55	0.81	0.030	3.7
C-3141	Cu	80	1.30	0.040	8.5

*The Ti liners were provided by the Rock Mechanics and Explosives Research Center and loaded by Jet Research Center.

TABLE XVI
 PENETRATION TESTS IN STEEL FOR JRC CHARGES

<u>Liner Material</u>	<u>Liner Angle (deg)</u>	<u>Standoff (CD)</u>	<u>Hole Diameter (in.)</u>	<u>Penetration (in.) (CD)</u>	
Cu	100	1.0	0.19	0.65	1.30
Cu	60	1.0	0.22	1.42	2.84
Al	100	1.0	0.31	0.30	0.60
Al	80	1.0	0.27	0.41	0.82
Ti	100	1.0	0.31	0.26	0.52

Data furnished by Jet Research Center

APPENDIX B

CALCULATIONS FOR SANDSTONE STANDARD

Oven Dried Sample

Index	P_1 (atmos)	P_2 (atmos)	$\frac{P_1 + P_2}{2}$	$P_1 - P_2$	Q (cc/sec)	$\frac{P_2}{\frac{P_1 + P_2}{2}}$	Q_{AVG*}	$\frac{Q_{AVG}}{A}$	$\frac{P_1 - P_2}{L}$
2.5	1.1774	1.0142	1.0958	0.1632	25.83	0.9255	23.906	2.238	0.0510
5.0	1.3418	1.0168	1.1793	0.3250	50.83	0.8622	43.826	4.103	0.1015
7.5	1.4866	1.0326	1.2596	0.4540	75.83	0.8197	62.158	5.820	0.1418
10.0	1.6326	1.0590	1.3458	0.5736	100.00	0.7868	78.680	7.367	0.1792
12.5	1.7668	1.0800	1.4234	0.6868	122.5	0.7587	92.94	8.702	0.2146
15.0	1.9274	1.1168	1.5221	0.8066	147.50	0.7337	108.22	10.132	0.2520

* Q_{AVG} is determined by

$$Q_{AVG} = Q \times \frac{P_2}{\frac{P_1 + P_2}{2}}$$

Klinkenberg Correction

$\frac{P_1 - P_2}{L}$	$\frac{Q}{A}$	\underline{K}	$\frac{1}{\underline{P}_m}$
0.1015	4.103	0.739	0.848
0.1418	5.820	0.750	0.794
0.1792	7.367	0.751	0.743
0.2146	8.702	0.742	0.703
0.2520	10.132	0.735	0.657

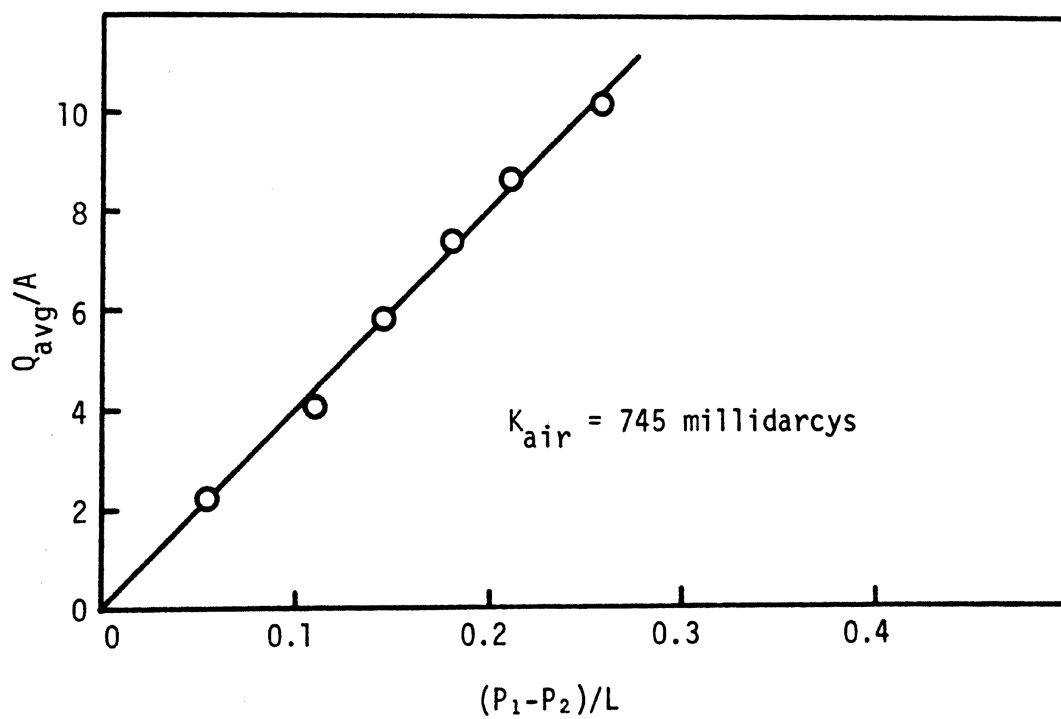


Figure 38. Permeability Curve for Sandstone

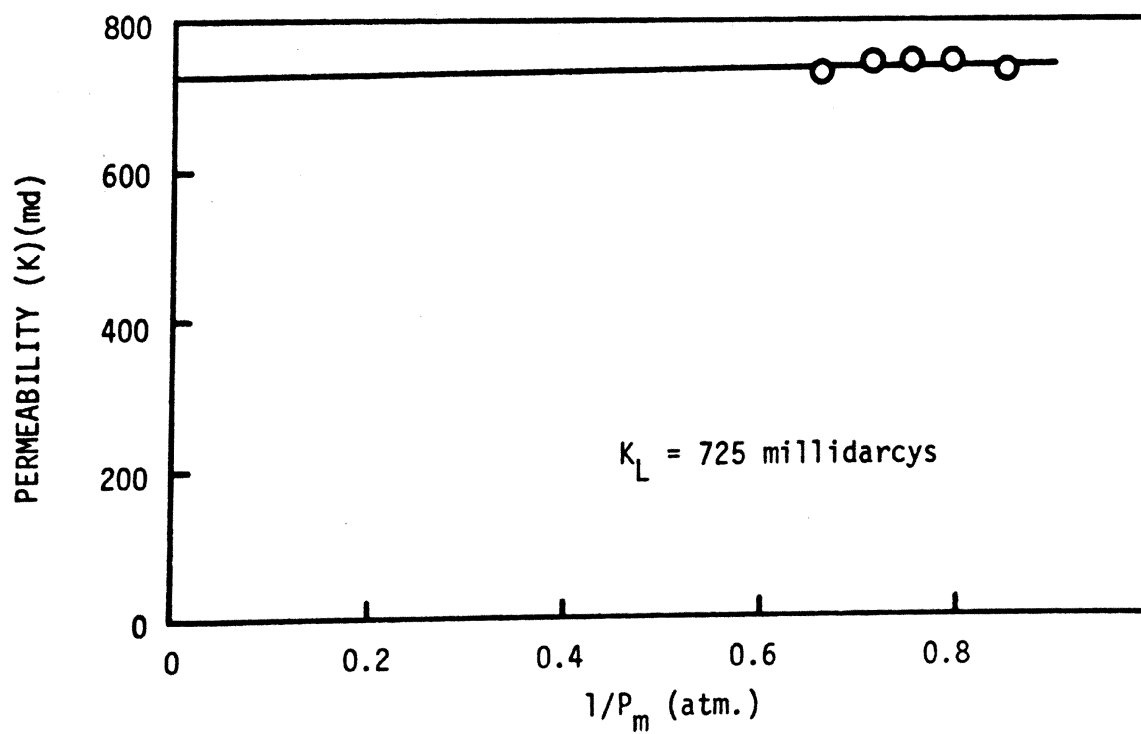


Figure 39. Klinkenberg Correction for Sandstone

APPENDIX C
MATERIAL PROPERTIES

Material	Longitudinal Velocity $\frac{\text{meters}}{\text{sec.}}$	Shear Wave Velocity $\frac{\text{meters}}{\text{sec.}}$	Tensile Strength $\frac{\text{dynes}}{\text{cm}^2} \times 10^8$	Specific Gravity	Shore Hardness Number	μ	$\frac{\text{dynes}^E}{\text{cm}^2} \times 10^{11}$
Air	335	--	--	0.012			
Water	1448	--	--	1.0			
Plexiglas	2683	1067	7.25	1.19	73.7	.40	.31
Dolomite	4451	2622	--	2.5		.23	
Coal	833* 1388**		0.345	1.10	68		
Brass	4700	2110	33.8	8.47		.37	10.3
Aluminum	6420	3040	25.0	2.82		.35	7.1
Copper	5010	2270	21.3	8.96		.37	11.2
Titanium	6070	3125	54.0	4.5	50	.32	11.6
Steel	5941	3251	27.6	7.8	27	.28	17.2
Lead	1960	690	1.77	11.34	12.9	.43	1.38

*perpendicular to bedding planes

** parallel to bedding planes

APPENDIX D

PROXIMATE ANALYSIS OF COAL FROM ILLINOIS NO. 6 SEAM

Analysis on Dry Basis

Ash	15%
Sulfur	0.7%
Volatiles	37%

Fixed Carbon Content = $100\% - (\text{Ash} + \text{Volatiles})$
= 48%

BTU Value 10.800

Analysis Data Furnished by Inland Steel, Sesser, Illinois